THESIS ON MECHANICAL AND INSTRUMENTAL ENGINEERING E43

Exothermically Synthesized B_4C-Al Composites for Dry Sliding

EDUARD KIMMARI

TUT

PRESS

TALLINN UNIVERSITY OF TECHNOLOGY
Faculty of Mechanical Engineering
Department of Materials Engineering

Dissertation was accepted for the defence of Degree of Doctor of Philosophy in Engineering on June 27, 2008

Supervisor: PhD Lembit Kommel, Faculty of Mechanical Engineering, Tallinn University of Technology

Opponents: DSc Boris B. Straumal, Professor at Moscow Institute of Steel and Alloys (Technological University), Moscow, Russian Federation

DSc Irina Hussainova, Senior Researcher at Department of Materials Engineering, Tallinn University of Technology, Tallinn, Estonia

Defence of the thesis: September 11, 2008, at 14:00
Lecture hall: V-215
Tallinn University of Technology
Ehitajate tee 5, Tallinn

Declaration:
Hereby I declare that this doctoral thesis, my original investigation and achievement, submitted for the doctoral degree at Tallinn University of Technology has not been submitted for any academic degree.

ISSN 1406-4758
ISBN 978-9985-59-842-9

OÜ*INFOTRÜKK*

MASINA- JA APARAADIEHITUS E43

Eksotermiliselt sünteesitud B_4C-Al komposiidid tööks liugehõõrdumise tingimustes

EDUARD KIMMARI

TUT

PRESS

CONTENTS

INTRODUCTION

Development of lightweight wear-resistant materials and cost-effective methods to produce them are challenges of great importance since provide resource savings and reduce energy consumption. From this point of view, the composites based on low density and wear-resistant boron carbide, including B_4C-Al offer a material system of interest.

The main problem associated with preparation of B_4C-Al composites is the high reactivity of the constituents at processing temperatures resulting in complicated microstructural control. Appropriate processing conditions can provide materials with exceptional properties tailorable through microstructural composition. Nevertheless, there are still uncertainties and inconsistencies between published experimental data related to interfacial chemistry and microstructural characterization because of different technologies used for the preparation of B_4C-Al composites. Another feature is that B_4C-Al composites as tribomaterials have drawn very little attention.

The manufacturing of B_4C-Al by conventional powder metallurgy routes requires prolonged high temperature processing and special equipment, which consume energy and time and make the production costly. Reaction-based processing methods are suitable to solve many problems associated with the fabrication of advanced engineering materials.

The present work concerns a B_4C-Al composite of selected ceramic and metal content synthesized by exothermic reaction. Microstructural designing of synthesized compacts via secondary thermal processing is proposed to produce the lightweight composites of high wear resistance in dry sliding conditions. Materials properties are characterized by means of the mechanical and tribological response.

Acknowledgements

I take this occasion to express my sincere gratitude to all those people who made this work possible.

First of all, I express my profound sense of gratitude to my supervisor, PhD Lembit Kommel for his guidance and support.

I am heartily grateful to all my colleagues from the Department of Materials Engineering and Materials Research Centre for support, assistance, and scientific discussions.

Doctoral School “New Production Technologies and Processes”, Tallinn University of Technology and Estonian Science Foundation (grants no. G5611, G6163 and G6660) are acknowledged for financial support and equipping.

Finally, I would like to thank my family and friends for their patience, encouragement and support throughout this work.

Author's contribution

The author of this thesis took part in sample preparation routine, was responsible for carrying out of the experiments, collecting, processing and further analysis of experimental data. The intellectual merit which is the result of the framework where the contribution of every author should not be underestimated.

Approbation

1. The 14th International Baltic Conference "Materials Engineering 2005", Kaunas, Lithuania, October 6-7, 2005.
2. The 12th Nordic Symposium in Tribology, NORDTRIB 2006, Helsingør, Denmark, June 7-9, 2006.
3. The 15th International Baltic Conference "Engineering Materials & Tribology" BALTMATTRIB - 2006, Tallinn, Estonia, October 5-6, 2006.
4. The 6th International DAAAM Baltic Conference INDUSTRIAL ENGINEERING, Tallinn, Estonia, April 24-26, 2008.

ABBREVIATIONS AND SYMBOLS

ASTM – American Society for Testing and Materials
as-synth. – as-synthesized
BPR – Ball-to-Powder Ratio
CMC – Ceramic Matrix Composite
CMV – Cumulative Mean Value
CTE – Coefficient of Thermal Expansion
EDS – Energy Dispersive Spectroscopy
GOST – Russian Organization for Standardization
HIP – Hot Isostatic Pressing
H_{IT} – indentation hardness
HB – Brinell hardness
HM – Martens hardness
HRA – Rockwell hardness
HV – Vickers hardness
IPC – Interpenetrating Phase Composite
ISO – International Organization for Standardization
MMC – Metal Matrix Composite
PCV – Percent Coefficient of Variation
OM – Optical Microscopy
rpm – rotations per minute
SEM – Scanning Electron Microscopy
SHS – Self-Propagating High-Temperature Synthesis
ss – steady-state
TRS – Transverse Rupture Strength
TUT – Tallinn University of Technology
wd – whole distance
XRD – X-Ray Diffraction
ΔG – free energy change of reaction
ΔW_E – percentage deviation of volumetric wear predicted by exponential model
ΔW_Y– percentage deviation of volumetric wear predicted by Yang’s model
μ – coefficient of friction
C – contiguity
E – elastic modulus
F – normal load
F_{f} – frictional force
h_{r} – residual depth (unrecoverable deformation)
L – sliding distance
P – porosity
v – sliding velocity
W – volumetric wear
W_{sp} – specific wear rate
W_{p} – indentation plastic work
W_{t} – indentation total work

1 REVIEW OF THE LITERATURE

1.1 Ceramic-metal composites

The composite material is a material that consists of two or more physically and/or chemically distinct, suitably arranged or distributed phases, with an interface separating them. The concept of composite material is to combine different materials to produce a new one with performance unattainable by the individual constituents [1].

Cermets, composite materials composed of ceramic (cer) and metal (met) have been utilized to solve technological problems for a long time but only in the 1960s did these materials start capturing the attention of industries. Composite materials have become common engineering materials and are designed and manufactured for various applications [2].

The nonmetallic chemicals usually increase the hardness, wear resistance, and heat resistance of composites. The metallic phase bonds hard particles into one composite material and provides strength and plasticity to cermets. Therefore, the properties of cermets depend on metal and ceramic phase properties, their proportion, and adhesion between initial components [3].

Implementation of cermets in engineering applications requires experience in designing with materials, design data, field performance data, and performance and failure prediction methods [4].

1.1.1 Composite materials – global trends

The development of **resource-savings materials** that help preserve energy and/or natural resources and **low-cost fabrication methods** are among the main trends declared in “A Vision of Materials Science in the Year 2020” [5]. Global energy consumption has been increased continuously year by year. In 2000 the world’s energy consumption was 1.8 times higher than in 1971 and in 2020 it is expected to be 1.4 times higher than in 2000 [5]. Thus, the development of lightweight materials and economical methods to produce them may provide energy savings and more effective utilization of non-reproducible resources.

One of the main steps in the advancement of materials processing is the achievement of a controlled and reproducible microstructure, and at the same time the composite material must satisfy with mechanical, chemical and economical criteria [6, 7].

1.1.2 Features of boron carbide-aluminum material system

The main reasons for focusing on boron carbide-aluminum composites are the light weight of constituents, extremely high hardness and stiffness of B_4C, and ductility of recyclable Al [8].

Thermodynamical, **chemical** and **physical compatibility** determine the interface phenomena and the capability of successful forming of boron carbide composite materials [9]. There are two main types of interaction occurred between a liquid and a solid phase: physical and chemical, where the bonding forces due to chemical interaction are up to three order higher than forces of physical nature [10].

The difference in **coefficients of thermal expansion** (CTE) is among the main problems of physical compatibility for composites of ceramic/metal system because of residual stresses due to CTE mismatch. The compositions with low CTE mismatch are generally preferable.

Wettability is one of the most significant properties determined by physical interactions. Proper wetting is an essential condition for the generation of a satisfactory bond between solid ceramic phase and liquid metal. The results of the works focused on wettability between boron carbide and aluminum suggest high contact angles (>100°) and poor adhesion (adhesion work <400 MJ/m^2), i.e. poor bonding for given ceramic/metal system under vacuum at temperatures below 1000 °C [9, 11]. Enhancement of wetting has been found in air due to formation of boron oxide B_2O_3 on the surface of boron carbide particles [12-14].

The chemical compatibility is a more complicated problem for boron carbide-aluminum. The strongly temperature-dependent **chemical reactivity** between Al and B_4C is the main factor determining the composition and properties of final material [15-19]. The achievement of the required interfacial bonding strength is feasible only due to controlling of complicated processes of wetting and chemical interactions both in liquid and in solid phase [9]. From this point of view, the understanding of phase equilibrium in Al-B-C system is a matter of great importance.

Works focused on the fabrication of B_4C-Al composites suggest that B_4C and Al do react in temperature interval 450-2300 °C; those reactions lead to the formation of binary and ternary borides and carbides of aluminum [12, 15, 20-26]. The possibility of chemical reaction between initial components is determined by change of free energy (ΔG) of a system. Smagorinski and Tsantrizos [27] have evaluated the free energy change ΔG for reaction (Eq. (1)) to be −193.6 kJ/mol at temperature of 298 K and at atmospheric pressure:

$$3B_4C + 5Al \rightarrow AlB_{12} + Al_4C_3 \qquad (1)$$

Thus, the reaction between aluminum and boron carbide is not only possible but exothermic in nature. In liquid state the reactivity remarkably increases [9].

Kara et al. [22] have developed a reaction model (Eq. (2)) for B_4C-Al system that gives good predictions for Al_3BC content in temperature range 985-1370°C and reaction duration times up to 2 hours:

$$4B_4C(s) + 13Al(l) \rightarrow 4Al_3BC(s) + B(Al) + AlB_{12}(s)\ (T>985\ °C) \qquad (2)$$

where (s) – stoichiometry, (l) – liquid.

Halverson *et al.* [24] have developed a reaction series map for B_4C-Al system (Fig. 1). The map presented in Fig. 1 illustrates the variety of reaction products formed under equilibrium conditions (X-phase nowadays reported as

Al_3BC). The phases presented in the map are in agreement with those reported in [15, 21, 28].

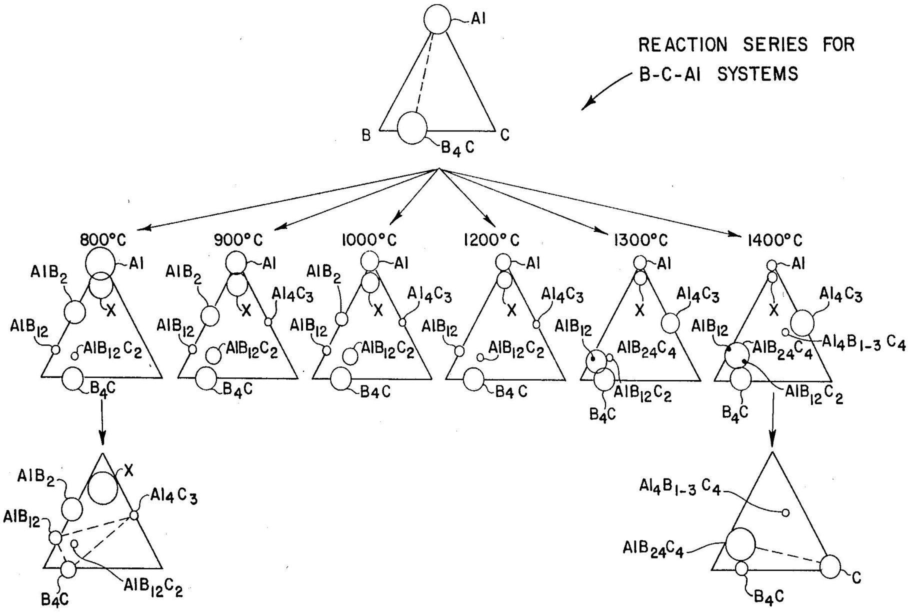

Figure 1. Reaction series map for B_4C-Al system [24]

Despite recent progress in B_4C-Al system characterization, significant problems remain in analysis of interfacial chemistry, controlling the quantity of each component, homogeneity achievement in final composite. Hitherto there is a fewness of the works on the B_4C-Al interface chemistry, and the results published by different authors are not in coincidence probably due to different fabrication and processing conditions [15, 21, 23, 25, 29, 30].

The reactivity between B_4C and Al at temperatures not exceeding 800 °C is slow and the only phases formed are Al_3BC and AlB_2 [9, 24]. At higher temperatures the reaction rates are so fast that control of microstructure to achieve desired composition becomes very complicated because of several unwanted phases form.

The formation of new phases is accompanied by depletion of aluminum [21]. Pyzik and Beaman [25] have studied the influence of temperature and duration of heat treatment on residual aluminum content in the 70 vol.% B_4C-Al (Fig. 2). The similar behavior has been found for powder blends and dense composites.

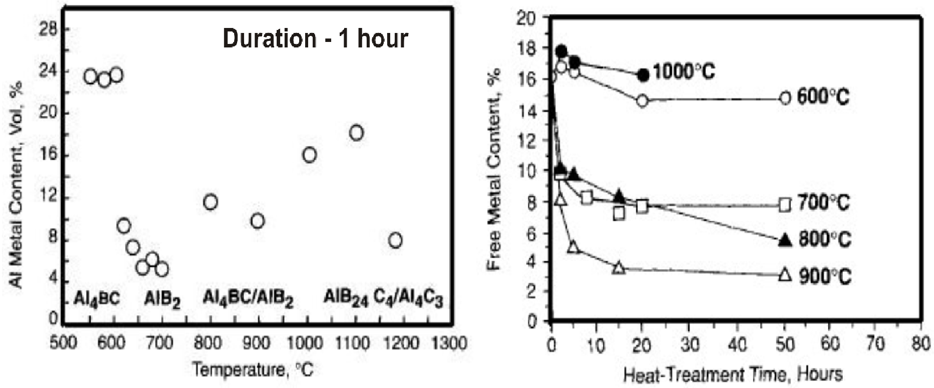

Figure 2. Effect of processing conditions on Al content in 70 vol.% B_4C-Al [25]

Review of scientific literature reveals that there is a series of publications and patents related to B_4C-Al material system available. These composites have different applications: tribological, structural, thermal, nuclear [9, 20, 31-34]. Thus, various fabrication routes have been elaborated to produce composites for particular application – hot pressing, sintering, pressure infiltration, casting, spray techniques [23, 29, 35-37]. Many of these methods require additional approaches to overcome the limitations associated with B_4C-Al composition. Recently developed techniques such pressureless infiltration, reaction bonding, SHS, and explosive consolidation allow overcome these limitations and reduce the processing time [38-41].

Infiltration, a widespread approach of B_4C-Al composites fabrication, requires high temperatures (2100-2300 °C) to prepare a porous boron carbide body by sintering in vacuum or inert atmosphere. Such a high temperatures cause intensive grain growth [9]. The use of dopants allow to reduce the sintering temperature to 1750-1900 °C, just as the hot isostatic pressing HIP (1700 °C) [41]. Halverson *et al.* [24] have shown that the uniform application of pressure provided by HIP resulted in accelerating the densification kinetics faster than the chemical reaction kinetics and elimination of stress-induced microstructural inhomogeneities. Chemical reactivity of B_4C-Al system may be also reduced by preliminary carbonization or thermal passivation of boron carbide surface [25, 42]. However, these processes require high temperatures, special atmospheres and equipment which make the production of B_4C-Al composites expensive.

Since the reaction between B_4C and Al is accompanied with heat release [27], there is the possibility of synthesis by exothermic reaction. Hence, it would be favorable to produce the composites by self-sustaining reaction which requires external heat input only for process initiation.

Kommel [40] has developed the process of fabrication of B_4C-Al composites by self-propagating high-temperature synthesis (SHS or exothermic reaction synthesis). This approach was used in present research.

1.1.3 Self-propagating high-temperature synthesis

Self-propagating high-temperature synthesis (SHS) invented by Merzhanov and co-workers in 1967 is a class of reaction-based production methods that has attracted considerable interest [43]. SHS or exothermic reaction synthesis is suitable for production of a wide variety of materials, including powders and near net-shape products formed from ceramics, intermetallics, and composites for applications ranging from structural to oxidation- and wear-resistant materials. SHS process exploits the heat-energy released by the exothermic reaction of raw materials via a self-sustaining combustion wave which propagates from one end of the specimen to the other [44]. The greatest advantage of producing materials by the SHS method is that long processing times in high temperature furnaces are not necessary [45]. The reaction may be initiated from the sample surface with a heat flux or by bulk heating in a furnace. Heating rate and grain size have found to be critical parameters to initiate self-sustaining reaction and to control the rate of its propagation [46, 47].

Composites obtained by SHS are generally porous [48]. Densification of hot combustion products via mechanical pressing may provide dense SHS-products [47, 48]. Several densification methods are investigated nowadays in order to realize the benefits of SHS: hot pressing, extrusion, rolling, impact forging [48]. SHS plus mechanical pressing was found to be an easy and inexpensive method to produce composite materials.

1.2 Processing/microstructure/property relationship

The properties of advanced materials are frequently determined by the microstructure, which in turn, developed during processing. In this connection, the processing/microstructure/properties relation is the focus of many research works.

1.2.1 Boron carbide-aluminum – tailorable microstructures

As it was considered earlier the investigated material system may produce a variety of phases [12, 15, 20-26]. Thus there is a great potential in microstructural design when deal with B_4C-Al composition. Depending on conditions of primary and secondary processing different types of microstructure can be tailored. When eliminate the reaction products, typical MMC or CMC two-phase matricial structure is attained [15, 19, 25]. A multiphase ceramic-metal composite with isolated or interpenetrated phases (see Fig. 3) can be tailored using suitable processing [15, 49].

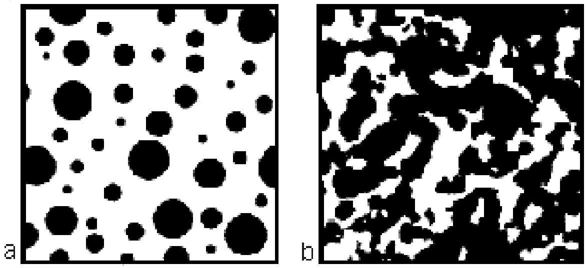

Figure 3. Schematic of possible B_4C-Al structures: a – matricial structure; b – interpenetrating interconnected structure [49]

According to Skorohod [50], multiphase materials may be classified into two categories: regular (ordered) and non-regular (disordered). Ordered systems are characterized by regular shape of constituents and spatial symmetry. Microstructural evolution is accompanied with change of relative volume fractions of initial components and in some cases with development of new phases. At the same time, porosity may outcome as a desired or side effect. The principles for microstructural control of porous and composite materials have been considered by Skorohod [50].

Most physical and mechanical properties are known to be structure sensitive. Thus, there is necessity for successful evaluation of microstructural parameters permitting to predict the effective properties if appropriate model exists.

Quantitative microstructural characterization of composite materials usually involves the measurement of binder mean free path, carbide contiguity, porosity, mean carbide size, and volume fraction of individual phases [51].

Overall, the properties of particulate-reinforced metal matrices depend on microstructural characteristics such as [36]:

- the size and shape of the reinforcing particle,
- the interparticle spacing,
- the volume fraction of reinforcement and metal,
- conditions at the matrix-reinforcement interface.

Recently much attention gained interconnected microstructure may be attained in B_4C-Al composites using several techniques, such as infiltration, SHS, or by secondary processing of particle reinforced composites. An interpenetrating phase composite (IPC) consists at least of two interconnected phases which construct a continuous network. This generation of composites possesses some properties that differ from those of traditional fiber- or particle-reinforced composites [52-55].

The microstructural characterization along with microstructure/property relationship of such class of disordered heterogeneous materials like IPC is in its infancy. Torquato [56] has described some approaches in microstructural characterization using statistical correlation functions on the example of three-phase B_4C-Al composite with an in-situ formed secondary ceramic phase. Other methods for IPC microstructural analysis have been proposed by Aldrich and Fan [57].

Relatively little work has been done on the determination of the effective properties of IPCs. It is more difficult to predict the effective properties of interpenetrating or co-continuous multiphase composite in comparison with the characterization of microstructures with well-defined inclusions such as whiskers, spheres or fibers [58]. Several proposals for characterization of B_4C-Al IPCs have been proposed by Torquato *et al.* [49] and Feng *et al.* [58, 59].

1.2.2 Effect of Al-B-C phases on mechanical properties

The phase composition and, hence, the mechanical properties of composites depend on processing variables. Because of at least nine binary and ternary compounds have been reported in Al-B-C system [24, 25], there is still no clear understanding of influence of each phase on mechanical response of B_4C-Al composites. Furthermore, the mechanical and physical properties of many individual phases of Al-B-C system are unknown. Pyzik and Beaman [25] have established that the main reaction products influencing the mechanical properties are Al_4BC, AlB_2, $AlB_{24}C_4$ and Al_4C_3.

One of the promptest and easiest means of characterization the mechanical behavior of materials is the measurement of hardness, i.e. by indentation technique. Strength properties, wear resistance, physical and thermomechanical properties have been correlated with hardness in many investigations. Depth-sensing indentation is a universal methodology for characterization of mechanical behavior of materials allowing the extraction of various parameters, including elastic parameters, recovery deformation, and energy-dissipation capacity [6, 60-62]. Table 1 represents the density and microhardness data for some Al-B-C phases.

Table 1. Properties of phases in Al-B-C system

Phase	Density, g/cm^3	Hardness, kg/mm^2
Al	2.70 [63]	125 (10 g load) [25]
B_4C	2.52 [63]	3220 (20 g load) [25]
AlB_2	3.17 [63]	1050 (10 g load) [25] 980 (100 g load) [25]
Al_4BC (1)	3.17 [63]	1400 (10, 20 g load) [25]
Al_4C_3	2.97 [63]	1250 (100 g load) [25] 1230 (300 g load) [25]
$AlB_{24}C_4$	2.37 [63]	2840 (20 g load) [25]
Al_3BC_3 (2)	2.66 [28]	1820 (Vickers, 50 g load) [28]

(1) earlier referred to as X-phase, nowadays - Al_3BC

(2) earlier referred to as $Al_8B_4C_7$

Several researchers have observed detrimental effect of high-temperature phases (Al_4C_3, $AlB_{24}C_4$, Al_3BC_3) on mechanical strength of B_4C-Al composites [25, 64, 65]. Pyzik and Beaman [25] have studied effect of Al-B-C phase equilibrium on hardness, flexure strength and fracture toughness of infiltrated B_4C-Al composites. In general, formation of harder reaction products leads to hardness improvement. The highest hardness and modulus were obtained in Al_4BC-rich samples (89 HRA); hardness of composites with a connected network of B_4C was found to be less sensitive to heat treatment. Flexure strength reduces with increase of heat treatment temperature and regardless which reaction product is formed (Fig. 4a). Higher fracture toughness exhibited samples contained AlB_2, while samples with Al_4BC and Al_4C_3 showed brittle behavior. Increasing of ceramic phase continuity reduces the toughness. Composites with isolated B_4C structure experienced higher fracture toughness as compared to those with connected B_4C structure (Fig. 4b).

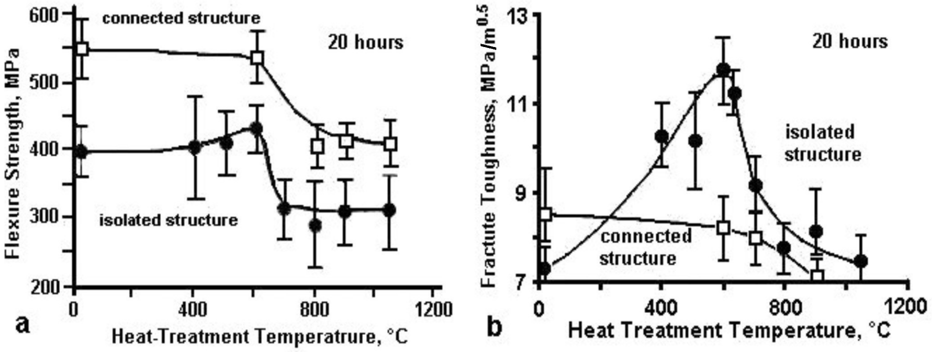

Figure 4. Effect of heat treatment temperature on flexural strength (a) and fracture toughness (b) of infiltrated B_4C-Al composites [25]

The interfacial zone between reinforcement and matrix is an essential part of composites. The strength of the interface is dependent on the nature of reinforcement (added or formed in-situ), on adhesion, and extent of the interfacial chemical reaction. Torquato *et al.* [49] have estimated the elastic and shear moduli for Al_3BC phase and the effective bulk and shear modulus for three-phase interpenetrating B_4C-Al composite. The effect of interfacial reaction extent on tensile properties has been studied by Kouzeli *et al.* [26]. Liu [66] has examined the effect of phases on thermal and electrical conductivity.

1.3 B_4C-Al as tribomaterial

Boron carbide is known as an exceptional wear-resistant material [67]. However, there is not so many published data relating to composites of B_4C-Al system as tibomaterial. The results of several researches suggest that B_4C-Al is a promising tribomaterial for sliding contacts exhibiting high wear resistance and stable smooth friction [31-33].

Tribological behavior of B_4C-Al composites has been studied by Chapman *et al.* [31] on the example of automotive brake pads fabricated from infiltrated composites with high volume fraction of B_4C (0.48 to 0.72). Results showed that these materials exhibit wear rates more than one magnitude lower than traditional semimetallic materials used for fabrication of brake pads, while friction coefficient values are within the industry standard range of 0.3-0.45.

The analysis of wear surface suggested that smooth friction and low wear was attributed to the development of interface glaze film.

Tribological behavior under dry sliding conditions of Al-alloy MMCs reinforced with boron carbide (3-12 vol.%) has been studied by Hemanth [32]. Two different predominant wear mechanisms were observed: adhesive severe (MMC with low B_4C content) and abrasive mild (MMC with high B_4C content).

Wear behavior analysis of plasma-sprayed AlSi-B_4C (0-25 wt.% B_4C) composite coatings performed by Sarikaya *et al.* [33] revealed plastic deformation and abrasion as the main failure processes under dry sliding.

Although the composites were tested under different operating conditions, it can be drawn from the works [31-33], that the wear mechanism is dependent on structure of composite. Composite materials with discontinuous ceramic phase (MMC type) generally show plastic deformation without cracking and, at the same time, boron carbide grains act as abrasive and plough into the counterface promoting material transfer [32, 33]. Composites with continuous ceramic phase showed mild tribochemical wear under conditions of dry sliding, when normal load is not high enough to cause cracking [31].

1.4 Friction and wear

Because the materials of interest are developed for dry sliding, a brief overview about friction and wear in general, and about sliding wear in particular is given below.

1.4.1 The complexity of wear processes

Tribology, which focuses on friction, wear and lubrication of interacting surfaces in relative motion, is a field of science defined in 1967 by a committee of the Organization for Economic Cooperation and Development [68]. Wear is the major cause of material wastage and loss of mechanical performance and any reduction in wear can result in considerable savings.

Wear can be classified into four primary types: sliding wear, abrasive wear, erosion, and corrosive wear [69]. Sliding wear is considered in this work further in more details since the materials of interest were found to be promising in sliding pairs [31, 67].

1.4.2 Sliding wear

Sliding wear occurs when solid surfaces are in sliding contact. Four predominant wear mechanisms exist when one solid surface slides over another one: **adhesion**, **surface fatigue**, **tribochemical reaction**, and **abrasion**. **Adhesion** is a very serious form of wear characterized by high wear rates and large unstable friction coefficients [68]. Most solids will adhere with another solid, while the extent of adhesion depends on: conditions of contact, atmosphere, types of materials in contact and their properties [68].

The formation of transfer films and/or transfer particles is the characteristic feature of adhesive wear. The rupture of adhesive junctions formed during sliding leads to material transfer. Transfer features can greatly modify the sliding characteristics promoting or suppressing wear [68].

Transfer particles generally cause the groove formation by ploughing as it is shown in Fig. 5a. Ploughing is a form of cutting leading to crack generation on the worn surface as a result of high tensile stresses [68]. When transferred material is present as a film or layer, low and smooth friction may result (Fig. 5b) [68, 70].

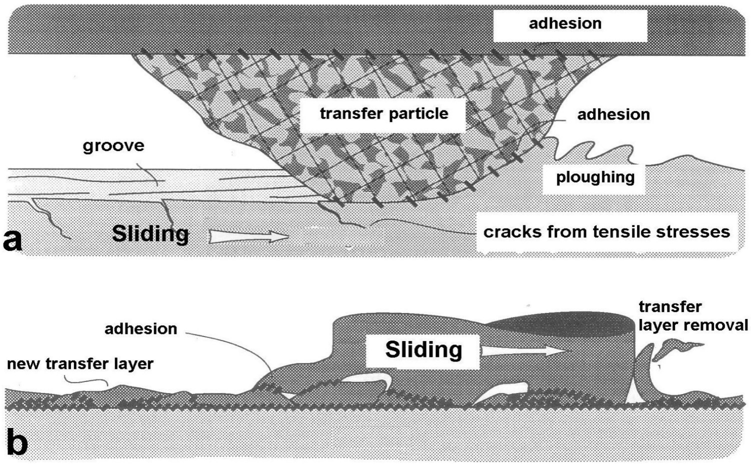

Figure 5. Effect of transfer particle (a) and transfer layer (b) [68]

The morphology and properties of these films vary depending on the properties of friction pair, environmental and operating conditions etc. The principles of formation of tribofilms and their role in friction will be discussed further in this section.

Surface fatigue or **fatigue wear** is caused by deformations of the asperities and surface layers at sliding interface. Contacts between asperities during sliding are accompanied by repeated high local stresses causing fatigue cracks initiation, propagation and fracture [68]. The process of debris formation by fatigue wear is described in [71]: a primary crack generally develops at the surface at some weak point and then propagates downward along weak planes (slip plane or dislocation cell boundary); then the crack reaches the surface by developing of a secondary crack or by connecting with some preexisting subsurface flaw.

Tribochemical reaction is the form of wear by formation of reaction products due to interaction between friction pair and environment. Generation of surface reaction layer, commonly designated **tribofilm** and composed of a mixture of the friction pair materials and oxidation products, plays an important role since it can be beneficial or harmful [68, 72]. Transfer film or third body layer is often present as a part of the tribofilm. Local transfer of material from one sliding component to the other can begin soon after sliding commences. Transfer occurs at some but not all asperity contacts. This begins a complex process that produces structurally and chemically modified material by mechanical mixing. At any given time, patches of this mixed material are distributed on the surface.

According to Biswas [73], the in-situ tribofilm formation may be classified into two categories: inadvertent (chemically, mechanically or physically beget) and deliberate. Zhou *et al.* [72] have explained the transfer phenomenon in ceramic/metal friction couples from the viewpoint of physical chemistry as a kind of adhesion, which can be quantitatively characterized by adhesive energy between solids. Generation of protective oxide films, which retains the mild and smooth wear, is the main feature in ceramic/metal and metal/metal sliding contacts existent in air or other oxygen containing atmosphere [68, 73]. The process of oxidation may be accelerated by high friction temperatures.

The formation and subsequent loss of oxide films is the common process of **oxidative wear**. The characteristic features of oxidative wear are smooth worn surfaces, small debris, and stable coefficient of friction [68]. At low operating temperatures the oxide films form rapidly on the surface of metals and greatly suppress adhesive wear, while at high temperatures oxidation resembles corrosion at its high rate and can cause increased wear.

Different mechanisms of transferred oxide layer removal are proposed. One of them is associated with the fatigue damage of layer after a certain number of contacts with counterface surface [74]; another approach explains the oxide layer removal by reaching a critical thickness at which the layer becomes too weak to withstand the load and frictional shear stress [68].

The growth of oxide layer can happen in two different ways: by rapid oxidation of asperity tips (when friction temperature is high enough), and by growing together of wear debris.

1.4.3 Wear quantification

In following are listed some variables most used for quantification of wear resistance [75]:

- wear – volumetric or mass loss, m^3 or g;
- wear rate – volume loss per unit sliding distance, m^3/m;
- specific wear rate – volume loss per unit applied load per unit sliding distance, m^3/Nm;
- wear coefficient – non-dimensionless variable estimated as specific wear rate multiplied by room temperature hardness.

According to Czihos [76], analysis of a tribosystem can be carried out by means of three-dimensional access taking into account functional, energy and material aspects.

Classical approaches give the wear volume as a function of the normal load and sliding distance. The Coulomb friction model establish the proportionality between the friction force and the normal load, thus there is correlation between frictional force and wear volume. From this point of view, the volume of material removed appears to be directly proportional to the energy dissipated by friction that can be calculated as the work of frictional force. The friction energy dissipates mainly through generation of wear debris, temperature effects, and the material transformation at the interface [77]. Energetic approach in wear data analysis becomes considerable attention since it allows comparing the experimental data obtained under different test conditions (test duration, normal load, sliding speed) because they affect the input of energy and the wear volume in the same way [77]. This, in turn, may contribute reproducibility of wear data, which remains among significant problem in understanding of tribological properties and their quantification, because of wide scatter of experimental results often reported by different authors examined the same materials under the same testing conditions.

1.5 Aims of the study

Numerous studies have been carried out by other authors in the field of aluminum composites reinforced with carbides, oxides and nitrides such as alumina, silica, silicium nitride, zirconia, and boron nitride.

Relatively little attention has been paid to boron carbide as a particulate reinforcement for aluminum and its alloys. Studies related to boron carbide-aluminum composites mainly concentrate on such production methods like infiltration, hot pressing and squeeze casting. The present research is focused on the composites derived by the reaction synthesis that propagates as an exothermic reaction (process also called as SHS).

The object of this work is the lightweight composite material of a given composition produced by the reaction synthesis using a patented technology [40] and developed by secondary thermal processing. The reactivity between boron carbide and aluminum is strongly temperature dependent [15]. Therefore, the composites of boron carbide-aluminum system may have compositions with a plurality of phases with different types of microstructure.

The purpose of the present research is to develop a number of heat treatment methods allowing to modify the synthesized body in order to produce a material with appropriate structure and properties suitable for dry sliding wear.

The effect of environment and temperature of post-densification heat treatment on the microstructural development, mechanical and tribological properties of B_4C-Al composites will be studied.

2 EXPERIMENTAL CONDITIONS

The composite materials studied in the present work were produced in Laboratory of Powder Metallurgy, TUT. Ceramic-metal composite material was synthesized using SHS-technology [40] from powders of aluminum and boron carbide B_4C.

In the present study composites with 52 vol.% of initial content of boron carbide were produced. The composition was chosen based on knowledge gained from [40] and in order to provide possibility to develop different types of microstructure.

2.1 Preparation and processing of composites

2.1.1 Characterization of initial materials

Boron carbide (GOST 5744-85) grinding powder (fraction 5.2-74.4 μm, average 17.3 μm) containing ~4.0 wt.% free carbon was chosen as ceramic phase. Aluminum powder (purity 99.95 wt.%) with spherical particles was used as binder phase. Some properties of boron carbide are listed in Table 2.

Table 2. Selected properties of B_4C

Property	Value
Density, g/cm^3	2.52 [78]
Melting point, K	2720 [9]
Hardness (Knoop, 100g), kg/mm^2	2900-3580 [9]
Fracture toughness, MPa/m$^{0.5}$	3.3 [78]
Young's modulus, GPa	445 [78]
Shear modulus, GPa	180 [9]
Thermal conductivity, W/(m·K)	26 [78]
CTE, 10^{-6}/K	4.78 [78]

Powder blends were prepared by attrition mixing and milling using an attritor designed in Laboratory of Powder Metallurgy and illustrated in Fig. 6.

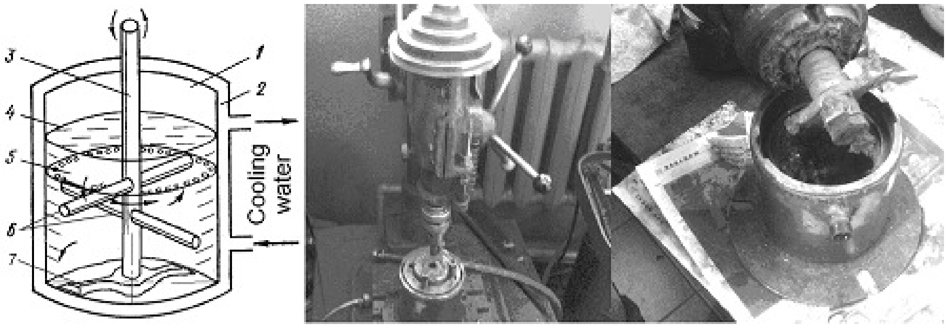

Figure 6. Scheme and photos of attritor: 1 – stationary drum space, 2 – water cooling jacket, 3 – shaft, 4 – milled powder, 5 – grinding media, 6 – arms, 7 – profiled blade

Boron carbide powders of different grain size were used in this research: the coarse-grained powder with average grain size of 17.3 µm and the fine-grained powder with average grain size of 1.24 µm. Particle size distribution analysis of initial powder grades is shown in Fig. 7. The fine grained boron carbide powder with specific surface area of 25 m^2/g was obtained using attrition milling during 6 hours at rotating speed of 800 rpm. The presence of B_2O_3 in milled powder was detected by XRD.

The powders were blended using tungsten carbide WC balls as grinding media with BPR (ball-to-powder ratio) 3:1 and ethanol as a solvent medium.

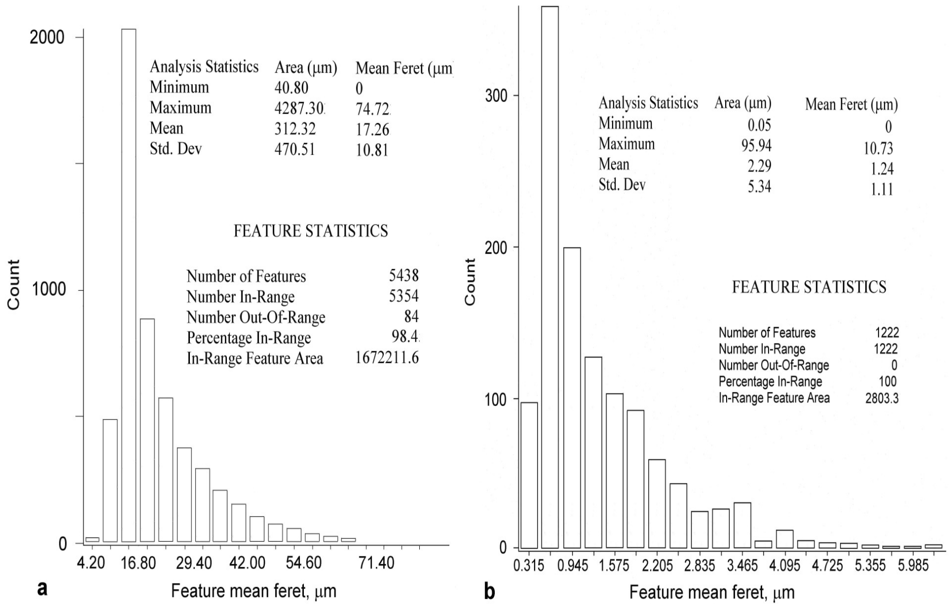

Figure 7. Histograms for the distributions of feret diameters for initial coarse (a) and attrition milled fine (b) boron carbide powder lots

2.1.2 Preparation and processing conditions

The prepared powder blend was dried at a temperature of about 100-150°C for 2 hours, then placed in a steel container with rectangular shape in plane (100×60 mm) and Cassinian oval cross-section (Fig. 8) and compacted by vibration.

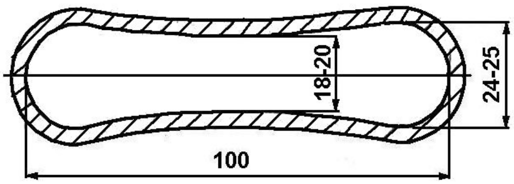

Figure 8. Schematic illustration of cross-section of steel container [40]

Heating the container with Al and coarse-grained B_4C powder mixture in a furnace up to a temperature of 1000±30 °C initiates the SHS process. When fine-grained B_4C powder is used the SHS starts at 750±20 °C. As a result of the exothermic reaction the temperature rises up to 1100-1150 °C [40]. Immediately after the SHS (at the liquid state of the binder), the steel container with composite material was uniaxially pressed at a compacting pressure of ~150 MPa. The most effective densification of boron carbide based materials is observed at the pressure 50-300 MPa; higher pressures cause exfoliation of compacts [9].

The SHS was completed in 10-15 seconds for the given composition and size of green body. Fig. 9 illustrates the composite fabrication process and shows an example of the microstructure of an as-synthesized composite.

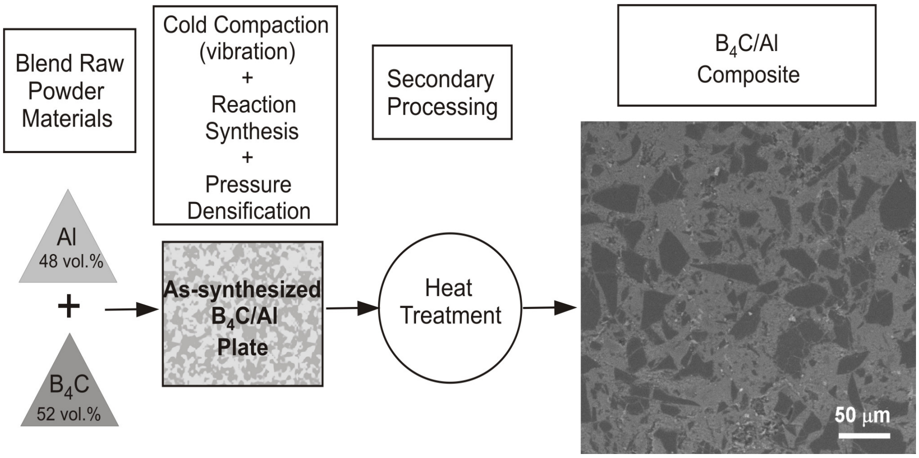

Figure 9. Composite fabrication process flow sheet

The temperature interval of heat treatment was selected to provide an improved wear resistance of the composites (as compared with that of as-synthesized). Previous studies [22, 24, 25, 28, 29, 37] state that regardless of manufacturing method the heat treatment applied to as-received B_4C-Al bodies leads to the depletion of the metallic phase, the formation of reaction products (binary and ternary carbides and borides) and, consequently, to changes in properties. Vacuum and air were chosen as treatment environments. Synthesized B_4C-Al bodies were placed in a graphite chest and in the air environment coated with a ZrO_2 flux bath.

Table 3 summarizes the conditions of secondary processing for B_4C-Al composites.

Table 3. Conditions for secondary processing of B_4C-Al

Regime	Temperature, °C	Atmosphere	Details
1	700	vacuum	heating rate ~250 °C/h, hold 15 min, cooling down to ~150 °C in furnace
2	1080	vacuum	same as regime 1
3	1150	vacuum	same as regime 1
4	1300	vacuum	same as regime1
5	1500	vacuum	same as regime1
6	1080	air+flux ZrO_2	heating rate ~200 °C/h, hold 15 min, cooling down to ~150 °C in furnace (~50 °C/h)
7	1470	air+flux ZrO_2	same as regime 6

2.1.3 Sampling

The samples for the present study were prepared in Laboratory of Powder Metallurgy and in Laboratory of Metallography (TUT). Primary mechanical processing of as-synthesized plates included diamond wheel grinding and cutting into specimens of required size with a Struers cutting machine.

Samples for metallographic observations were encapsulated into plastic using a hot mounting machine Struers Prestopress-3 and polished using Struers Pedemax-2 apparatus including last stage of polishing by 1 μm diamond paste.

2.2 Characterization approaches and equipment

2.2.1 Microstructural characterization

Microstructural characterization of the composites was performed using optical microscopy OM (Nikon CX) and scanning electron microscopy SEM (Gemini LEO Supra 35, JEOL JSM-840A, and Hitachi TM1000) equipped with energy dispersive spectroscopy (EDS). X-ray diffraction (XRD) was performed with a Siemens Bruker D5005 analyzer with CuKα-radiation (scanning range 2θ from 20° to 80° with step of 0.04°). Changes in B_4C-Al composition were characterized by the ratio of peaks intensity of crystalline phases, which was determined by measuring the intensities of the three characteristic non-overlapped diffraction lines and comparing the obtained result from one grade to another.

The microstructures of the composites were quantified in terms of the ceramic phase contiguity C and porosity P. JMicroVision [79] software was used for image analysis. Contiguity of ceramic phases was evaluated by the linear intercept method. Porosity level and relative amount of phases were determined using the point counting method. Eight image fields (1000×1000 μm) for each sample were analyzed to evaluate an arithmetic mean value.

2.2.2 Mechanical characterization

Mechanical characterization of B_4C-Al composites was done by means of indentation and bending testing. Indentation hardness measurement is the simplest and widely used method for mechanical characterization, although the results are not absolute and depend on test methodology [80]. Instrumented indentation has been found to be an attractive method for hardness and elastic properties measurement of engineering materials, providing online data computerized recording [62, 81, 82]. Zwick 2.5/TS1S indentation machine equipped with a Vickers indenter was used for the instrumented indentation according to the standard EN ISO 14577-1 [83] (load 98 N, dwell time 10 s). Elastic modulus E and indentation hardness H_{IT} were determined from load-displacement curves in accordance with the Oliver-Pharr approach [62].

The bulk Vickers hardness was measured using Indentec 5030 SKV at load of 98 N (10 kgf), providing indentation over a number of grains, according to ISO 6507 [84]. At least eight indentations were done for each experimental point evaluation.

Because the materials of interest are multi-phase, non-homogeneous and prone to cracking, macro-hardness measurements may be highly variable and will not identify individual surface features. Microhardness of B_4C-Al composites was measured according to the ASTM E384-05 [85] standard test method. Buehler Micromet-2001 tester with the Vickers indenter was used, and up to 20 measurements performed for mean value calculation. A load of 50 gf was experimentally determined as providing no cracking of grains.

Three-point bending was performed with rectangular test-pieces using Instron 8516 according to ISO-3327 [86] at room temperature and a constant cross-head speed of 0.5 mm/min. Each data point for transverse rupture strength (TRS) represents the mean of 5-7 measurements.

2.2.3 Tribological characterization

Wear tests were performed on a block-on-ring apparatus at room temperature and without lubrication. According to the standard test method ASTM G77 [87], the stationary sample was pressed with a certain load to the cylindrical surface of a rotating steel disk (Fig. 10).

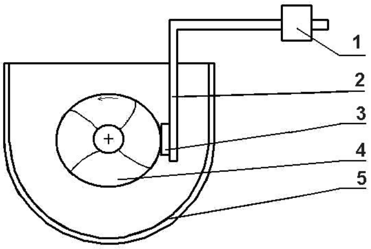

Figure 10. Schematic of sample arrangement for block-on-ring: 1 – load, 2 – lever arm, 3 – specimen block, 4 – rotating disk, 5 – chamber

The testing device included a rotating shaft to which a steel disk was fixed. The disk was nominally 178 mm in diameter by 13 mm width. The shaft was driven by an electric motor through a gear reducer. The specimen holder with a positioned specimen was attached to the lever arm to which a weight was added to enable force be applied along the horizontal diameter line of the disk and a required load value be obtained. The position of weight on the lever arm was determined by the calculation of the moments acting around the pivot point for the lever arm. The value of the load developed was then controlled by a dynamometer.

Test conditions were as follows: room temperature, atmospheric pressure, a constant relative humidity of 40±5 %, a linear velocity of 2.2 m/s (disk rotation speed of 235 rpm), normal loads of 40, 82 and 150 N, sliding distances of 1000, 2000, 4000, 6000 and 8000 m. The material of the disk was carbon steel (0.45 wt.% C) with a hardness of 200 HB. The blocks of the composite materials with dimensions of 20×12×6 mm were prepared by emery grinding to achieve uniform surface conditions.

Volumetric wear loss of the blocks was calculated using the weight differences of the thoroughly cleaned samples before and after the test measured with a digital balance to the nearest 0.1 mg. The mean value of three tests was taken as an experimental result.

The wear was quantified by means of the specific wear rate, i.e. volumetric loss per unit sliding distance per unit applied load.

Frictional temperature and the coefficient of friction were recorded continuously through the test. The temperature of both contacting and opposite surfaces of the block was continuously measured using an infrared thermometer and a thermocouple tightly clinging to the specimen's surface. The values of the friction coefficient were obtained by monitoring the tangential friction force.

The wear rate values predicted using two models were evaluated and compared with the experimental data. The equation (Eq. (3)) for the first model is an exponential equation derived from an assumption that the volume of material removed per unit sliding distance is proportional to the volume of the material available at the junctions [88, 89]. Further this model is called as exponential model.

- Exponential model [88, 89]:

$$W = \exp(-BL + C) \tag{3}$$

where W – volumetric wear, mm^3; L – sliding distance, m; B and C – empirical constants.

Another model is a modified Archard's model [90] proposed by Yang [91]:

- Yang's model:

$$W = A\exp(-BL) \tag{4}$$

where W – volumetric w×ear, mm^3; L – sliding distance, m; A and B – empirical constants.

2.3 The materials tested

The materials tested were the reaction bonded B_4C-Al composites subjected to the secondary thermal treatment at different processing conditions that are summarized in Table 4. The bulk densities of the specimens were measured by the Archimedes method. Additionally the conventional TiC- and WC-based composite materials produced in the Laboratory of Powder Metallurgy (TUT) were tested for comparison of dry sliding performance.

It should be noted that in the synthesis of composites from fine-grained powders difficulties occurred because in most cases highly activated powder mixture just burned out during heating up to the temperatures of synthesis. However, some preliminary results related to fine-grained composites are reported in the present research.

Table 4. List of materials tested (percent coefficient of variation in parentheses)

	Grade symbol	Bulk density, g/cm^3	Average grain size of initial B_4C, µm	Secondary processing	
	C0V	2.5 (2.7)	17.3	as-synthesized	COARSE
VACUUM	C700V	2.4 (4.8)	17.3	regime 1	
	C1080V	2.3 (8.7)	17.3	regime 2	
	C1150V	2.4 (6.0)	17.3	regime 3	
	C1300V	2.1 (9.3)	17.3	regime 4	
	C1500V	2.1 (8.8)	17.3	regime 5	
AIR	C1080A	2.6 (3.2)	17.3	regime 6	
	C1470A	2.4 (4.7)	17.3	regime 7	
	F1080A	2.5 (4.0)	1.24	regime 6	FINE
	F1470A	2.4 (3.3)	1.24	regime 7	

3. RESULTS AND DISCUSSION

3.1 Microstructure control

3.1.1 Vacuum heat treatment

The microstructural evolution of coarse-grained B_4C-Al composites as a result of secondary heat treatment processing in vacuum is presented in Fig. 11.

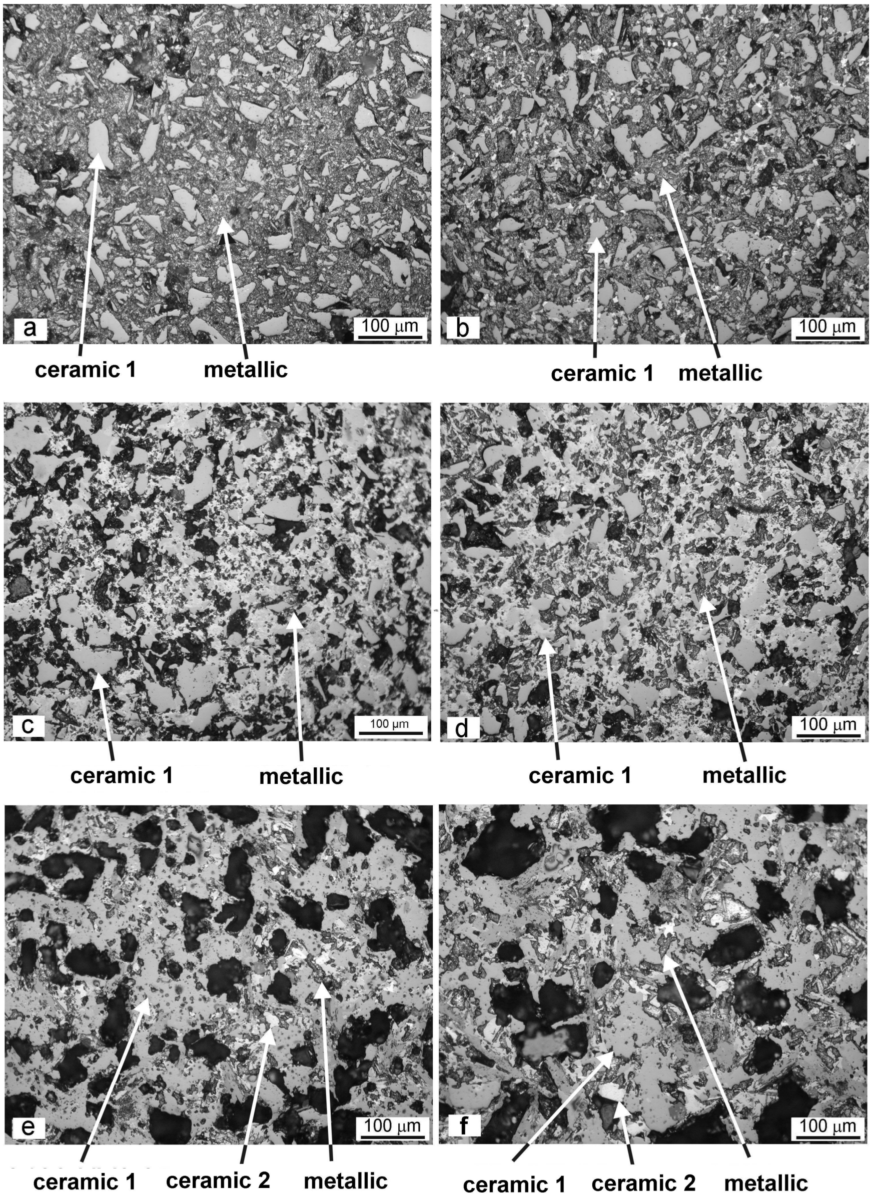

Figure 11. Microstructures of B_4C-Al composites: a – C0V, b – C700V, c – C1080V, d – C1150V, e – C1300V, f – C1500V

In Fig. 11 the main ceramic phase is in light-grey (further referred to as 'ceramic 1'), while the binder is in dark-grey color. Fig. 11a shows the microstructure of the material in as-synthesized condition that consists of an Al-matrix with distributed B_4C particles and graphite inclusions of black color.

The material subjected to the secondary processing (Fig. 11b-f) contains the phases generated by the reaction between Al and B_4C. The in-situ phases form the bridges between B_4C grains and thus develop a continuous heterophase ceramic skeleton. The microstructure of the composites heat-treated at temperatures 1080 °C and 1150 °C (Fig. 11c and d) can be characterized as composed of two interpenetrating co-continuous metallic (dark-grey) and ceramic (light-grey) networks and voids (black areas). Processing at higher temperatures leads to the formation of ceramic matrix structure with islands of residual metallic phase (Fig. 11e and f). The new ceramic phase of white color (Fig. 11e and f) is formed as a result of heat treatment at temperatures of 1300 °C and 1500 °C. This phase will be further designated as 'ceramic 2'. The connectivity of ceramic phases and the content of residual binder vary with the temperature of heat treatment. Fig. 11 allows for a conclusion that different types of microstructure can be tailored through secondary processing as long as there is enough residual binder for reactions. High porosity (black areas in Fig. 11b-f) and significant weight loss (see Table 4) result from vacuum heat treatment as a side effect because of the evaporation and outflow of Al and because of the formation of reaction products with higher density than that of initial components (see Table 1). Contamination of furnace interior sidewall with Al and drops of Al on the surface of composite samples reveal outflow and evaporation of metal.

Secondary heat treatment processing in vacuum is characterized by high reactivity of initial components resulting in the formation of reaction products of Al-B-C system, some of which have detrimental effect on strength [25]. Thus, in a vacuum environment chemical processes prevail over wetting processes. Another problem is that residual aluminum tends to evaporate causing a high level of porosity and void fraction. This is because of higher vapour pressure of Al than that of the vacuum environment [21].

3.1.2 Heat treatment in air

Heat treatment in air makes the presence of oxygen possible in the processing atmosphere. Very high oxygen affinity of Al along with high free energy of Al_2O_3 makes the presence of alumina in liquid Al unavoidable without special treatments [14]. The presence of oxide layers on B_4C and liquid metal surfaces changes the wettability and suppresses reactivity. The enhanced wettability was found to be through liquid-liquid reaction when B_2O_3 (melting point 450 °C [9]) contacted with liquid Al resulted in the formation of $B_2O_3{\cdot}Al_2O_3$ oxide compound [13, 14, 92]. Atmospheric pressure of the air environment is high enough to overcome the vapour pressure of Al at temperatures of heat treatment [93]. It was experimentally determined that the outflow of molten Al from the compacts during treatment is suppressed to a greater extent when a ZrO_2 flux bath is used instead of TiC or without any fluxes.

The microstructural evolution caused by heat treatment in air is shown in Fig. 12, where the boron carbide grains and binder appear black and grey, respectively.

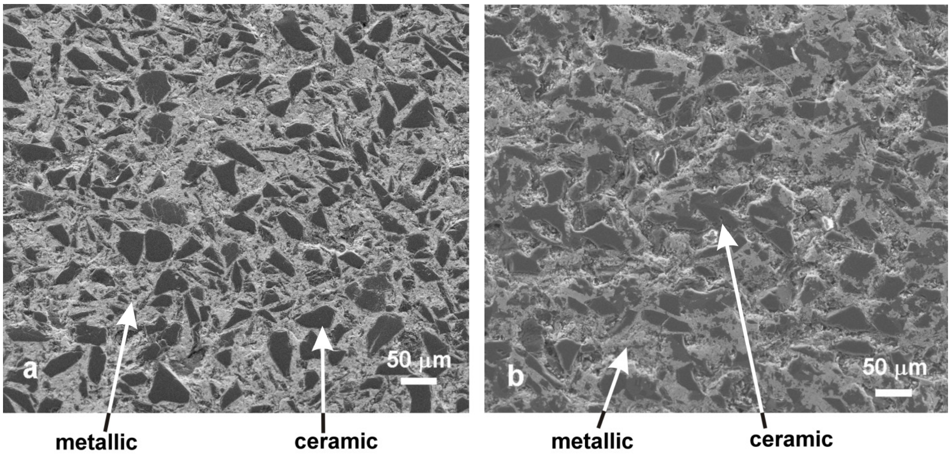

Figure 12. SEM micrographs showing synthesized B_4C-Al before (a) and after (b) heat treatment in air at 1080°C (b)

Higher density is an obvious distinguishing feature of material heat-treated in air as against to that processed in vacuum. In the sample C1080A (Fig. 12b) in some areas the reaction products have already formed a spatial quasi-continuous reaction zone (Fig. 12b, dark-grey areas). Boron carbide grains which are still in direct contact with Al are present as well. The microhardness of binder increased as a result of heat treatment because of a higher content of dispersed reaction products.

The relative content of ceramic and metal phases was determined using the point-count analysis of SEM micrographs performed using a multiphase image analysis software JMicroVision. The 2-D porosity was quantified in a similar manner. The concept of contiguity proposed by Gurland [57] was used to characterize the connectivity of ceramic phases in composite. The measurement of contiguity of the ceramic phases by the linear intercept method was subjected to some error because of difficulties experienced in inspecting the interfaces in heat-treated samples. However, the obtained results clearly indicate a change in the connectivity of ceramic phases. Table 5 summarizes the quantitative characteristics of B_4C-Al grades.

Table 5. Quantitative microstructural characterization of B_4C-Al composites

Grade	Ceramic Phases Content		Metal Phase Content		Ceramic contiguity		Porosity		
	CMV %	PCV %	CMV %	PCV %	CMV	PCV %	CMV %	PCV %	
C0V	50.7	8.8	46.9	6.4	0.147	3.4	2.4	7.0	
C700V	52.7	6.7	40.9	5.3	0.282	6.7	6.4	14.8	VACUUM
C1080V	60.8	9.8	18.0	10.5	0.597	7.0	21.2	8.3	
C1150V	60.6	7.8	19.9	14.9	0.603	9.5	19.5	8.9	
C1300V	67.0	5.6	3.4	7.4	0.775	3.5	29.6	7.6	
C1500V	60.7	3.3	11.6	6.9	0.779	6.2	27.7	6.8	
C1080A	63.7	3.8	33.2	4.1	0.446	4.4	3.1	14.1	AIR
C1470A	66.8	7.6	17.6	8.8	0.610	8.3	15.6	13.3	

CMV – cumulative mean value; PCV – percent coefficient of variation

It is obvious that ceramic content and its contiguity increase with the temperature of vacuum heat treatment increasing from 700 °C up to 1300 °C. Further increase in the temperature up to 1500 °C results in a decrease of the total content of ceramic phases from 67 % down to about 61 %. At the same time Al content increases from 3.4 % up to 11.6 %. The 2-D porosity from the point-counting method varies between 6.4 % and 29.6 % for samples heat-treated in vacuum. Composites heat-treated in air at 1080 °C had 2.5-4.0 % residual porosity. Heat treatment in air provides higher residual metal content and a lower voids fraction than vacuum heat treatment at the same temperature. This is explained by the suppressed evaporation of Al and lower reactivity of the components.

As it was mentioned previously, powder mixture contained mechanically activated fine-grained B_4C in most cases been burned out when heated up to the temperatures of the exothermic synthesis.

The microstructures of the composites synthesized from fine-grained boron carbide powder are shown in Fig. 13, where the dark-grey phase is the binder and the light-grey are ceramic phases. Areas of black color are the pores.

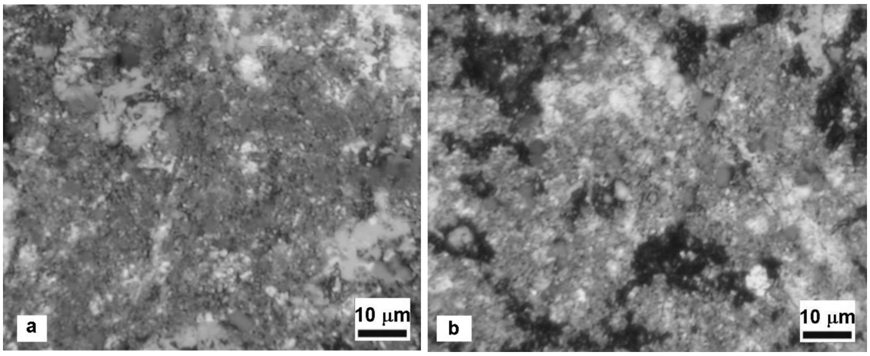

Figure 13. Microstructures of grade F1080A (a) and grade F1470A (b)

Heat treatment of B_4C-Al composites synthesized from fine-grained boron carbide powder cause the formation of reaction products (light phases) which tend to growth and clustering. Grade F1470A showed higher porosity than grade F1080A. No detailed microstructural characterization of fine-grained composites was performed due to difficulties associated with metallographic preparation and image analysis.

3.1.3 Al-B-C phases formed in situ

The results of XRD analysis suggest the formation of new phases as a result of secondary processing. Figs. 14 and 15 along with Table 6 summarize the phases identified by XRD.

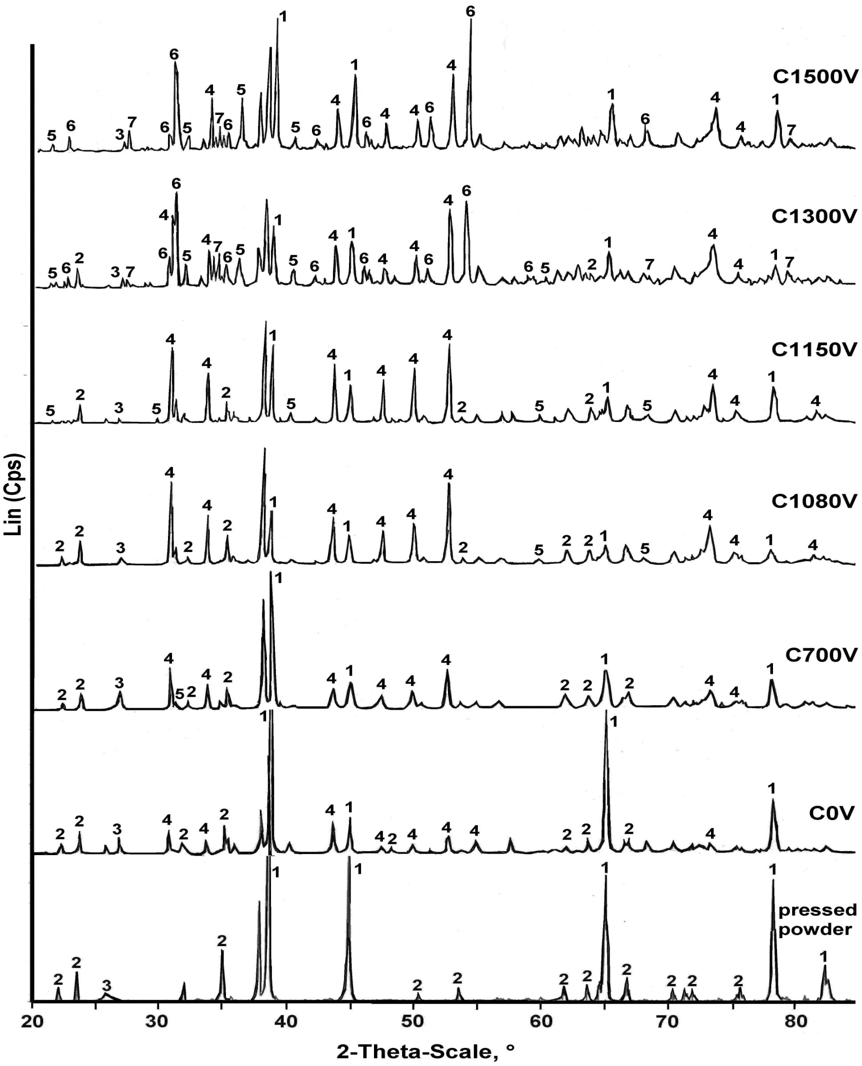

Figure 14. XRD patterns for B_4C-Al grades: 1 – Al, 2 – B_4C, 3 – C, 4 – Al_3BC, 5 – Al_4C_3, 6 – Al_3BC_3, 7 – AlB_2

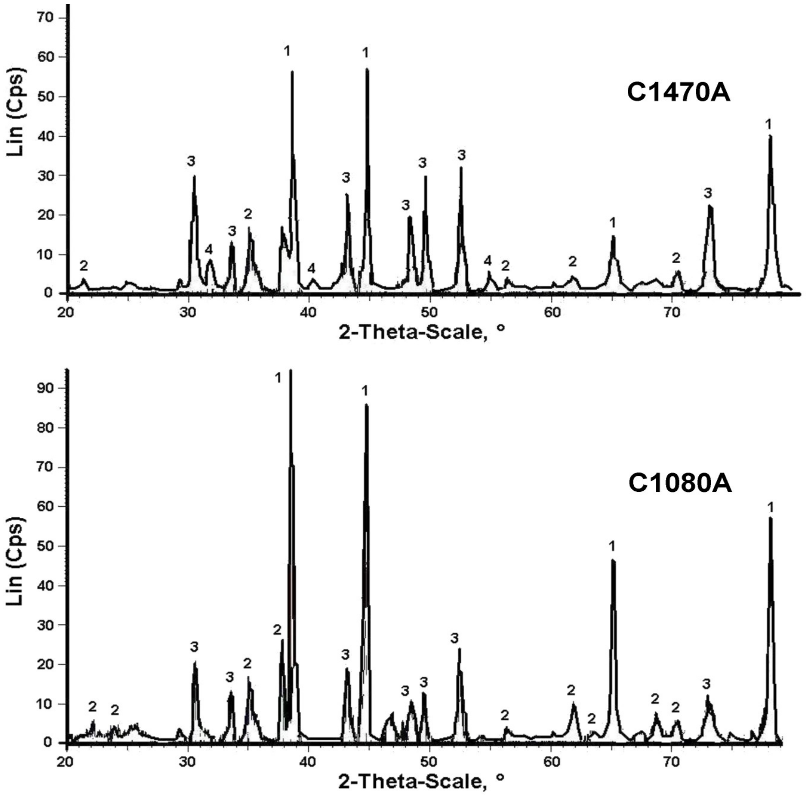

Figure 15. XRD patterns for C1080A and C1470A: 1 – Al, 2 – B_4C, 3 – Al_3BC, 4 – Al_4C_3

Table 6. Phases identified by XRD

Grade	Reactants	Reaction Products	
Powder	Al, B_4C, C		
C0V	Al, B_4C, C	Al_3BC	
C700V	Al, B_4C, C	Al_3BC	VACUUM
C1080V	Al, B_4C, C	$Al_3BC > Al_4C_3$	
C1150V	Al, B_4C, C	$Al_3BC > Al_4C_3$	
C1300V	Al, B_4C, C	Al_3BC, Al_4C_3, AlB_2 (weak lines), Al_3BC_3	
C1500V	Al, B_4C, C	Al_3BC, Al_4C_3, AlB_2, Al_3BC_3	
C1080A	Al, B_4C, C	Al_3BC	AIR
C1470A	Al, B_4C, C	$Al_3BC > Al_4C_3$	

XRD suggests that heat treatment in an oxidizing atmosphere leads to a lower number of reaction products than that in vacuum at the same temperature. No reflections from Al_4C_3 were found in sample C1080A as distinct from C1080V.

Al_3BC was found to be the main reaction product present in all bulk samples independent on the processing conditions. This is in agreement with the results stated by other researchers [15, 21, 22, 24, 25]. Al_3BC is known to precipitate at the B_4C-Al interface and the formation of this phase was found to be the reaction rate controlled [22].

The second reaction product identified by XRD Al_4C_3 starts reflecting weak lines in samples heat-treated in vacuum at the temperature of 1080 °C. The presence of this phase in the composites has been found to have a detrimental effect on the mechanical properties and may cause degradation of long-lived parts [25, 94, 95]. The same effect was observed in the present research. B_4C-Al heat-treated in air at 1470 °C revealed signs of spontaneous disintegration after a period of about two years since they were processed. Aluminum carbide Al_4C_3 is known to be unstable and hygroscopic, thus it reacts with water and atmospheric moisture [96] causing degradation of the composite. This phenomenon gives a possibility for disintegration of B_4C-Al by hydrothermal processing.

AlB_2 was observed in samples heat-treated in vacuum in a temperature range of 1300-1500 °C. This is in disagreement with [22, 24, 25], where the formation of AlB_2 was observed at temperatures below 1000 °C. The absence of this phase in samples heat-treated at lower temperatures is probably due to insufficient hold at the temperature range required for a diffusion rate controlled formation of AlB_2 [22]. The formation of AlB_2 phase at temperatures above 1423 °C has been observed by Solozhenko *et al.* [97]. Incongruent melting of Al_3BC results in formation of Al_3BC_3, AlB_2 and Al according to the following reaction [97]:

$$3Al_3BC \rightarrow Al_3BC_3 + AlB_2 + 5Al \quad \text{(at temperatures above 1423 °C)} \qquad (5)$$

Taking into account the results of the microstructural analysis (Table 5, metal content for C1300V and C1500V) and the XRD analysis (Fig. 14), it appears that there is a similar behavior of Al release.

The formation of in-situ phases is accompanied with the depletion and decomposition of initial components [15, 21, 25], which is implied by the plots in Fig. 16. The values were evaluated from the intensities of characteristic XRD lines of respective phases, giving a number that is the percentage ratio of the intensity of portions of the XRD pattern of the sample to intensity of the corresponding portion of the pattern of a reference (pressed powder).

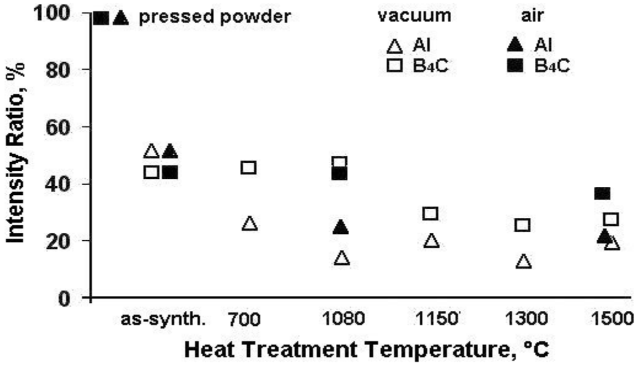

Figure 16. Percentage ratios of the peaks intensity of reactants in B_4C-Al grades

According to Fig. 16, Al reflection intensity starts to decrease at the lowest temperature of interest, i.e. at 700°C. This phenomenon implies the formation of Al-rich phase Al_3BC. A drop in the intensity of B_4C is observed at the temperature of 1150°C, suggesting an acceleration of decomposition of this phase.

Additionally, compositional changes were characterized through the analysis of maximal non-overlapped peaks intensity of the identified phases related to boron carbide peaks intensity of the same XRD-line. Changes in the intensity ratio of the reactants with the temperature of vacuum heat treatment are shown in Fig. 17.

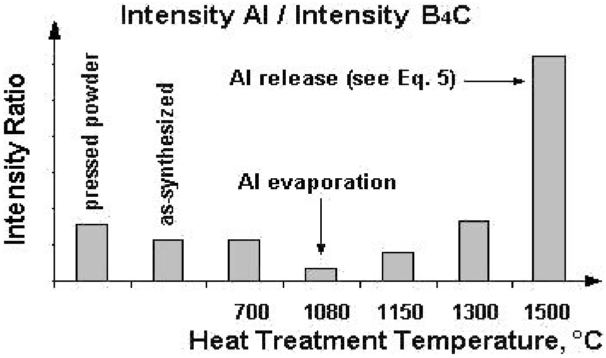

Figure 17. Ratios of peaks intensity of reactants – vacuum heat treatment

From Fig. 17 it follows that at temperatures below 1150 °C depletion of aluminum is the main process. Drop in relative intensity at 1080 °C indicates the intensification of depletion due to evaporation, which was confirmed by the contamination of furnace interior sidewalls by Al and by the presence of Al drops on the surface of heat-treated samples. Starting at 1150 °C dissolution of B_4C is predominant process associated with initial components because of Al deficit. A significant increase of Al relative intensity was observed at 1500 °C. This is associated with the decomposition of Al_3BC, as described earlier in this section (see Eq. (5)).

Fig. 18 shows the intensity ratio change of reactants for grades heat-treated in air.

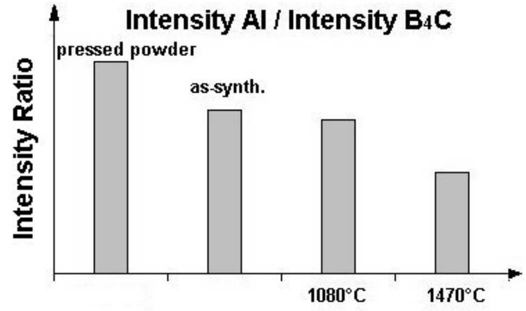

Figure 18. Ratios of peaks intensity of reactants – heat treatment in air

In contrast to Fig. 17, there is no drop of intensity ratio at 1080 °C. Taking into account the porosity and ceramic content for grades C1080V and C1080A (see Table 5), it can be concluded that high fraction of voids in vacuum heat-treated samples is caused to a greater extent by Al evaporation.

Fig. 19 confirms the higher reactivity of components in vacuum, resulting in a higher relative intensity of the reaction product Al_3BC. The presence of oxygen in the air environment suppresses reactivity [24]. This plot also indicates a higher rate of boron carbide dissolution and Al_3BC formation in the samples heat-treated in vacuum as compared with those heat-treated in air.

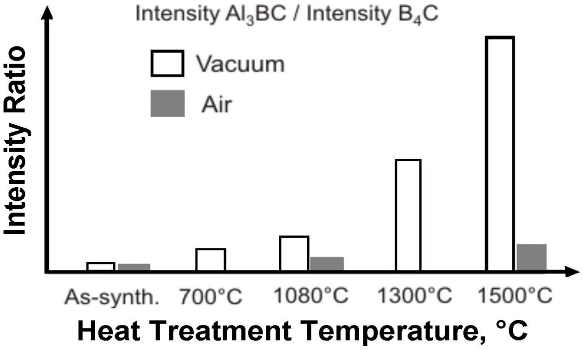

Figure 19. Ratios of peaks intensity of Al_3BC

3.1.4 B_4C-Al interfacial evolution

Interface evolution was analyzed by an example of the composites synthesized from coarse-grained boron carbide powder and heat-treated in air. Fig. 20a, b and c show the microstructures of the as-synthesized composite, grade C1080A and grade C1470A, respectively.

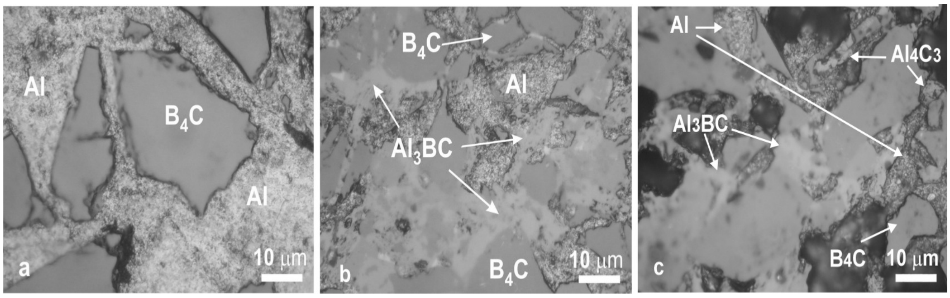

Figure 20. Interfacial transformation in B_4C-Al: a – as-synthesized, b – heat-treated at 1080°C, c – heat-treated at 1470°C (heat treatment in oxidizing atmosphere)

As it was established, the main phase developed at B_4C-Al interface is Al_3BC. XRD analysis (Fig. 14) suggests some presence of Al_3BC in an as-synthesized material, although visually this phase is not distinguished (Fig.

20a). As a result of heat treatment the crystals of Al_3BC starts forming at B_4C-Al interfaces. When the temperature of heat treatment increases up to 1080 °C, a quasi-continuous ceramic zone is developed (Fig. 20b). Further heating causes a detrimental Al_4C_3 to be formed and voids to arise.

It was found that the formation and growth of Al_3BC are responsible for the development of a continuous ceramic skeleton. Interfacial phenomenon was analyzed by means of SEM and EDS. Fig. 21 shows intensities of elements along a straight line in an interfacial zone of grade C1080A. Additionally, SEM mapping of elements was performed to clarify element distribution (Fig. 22).

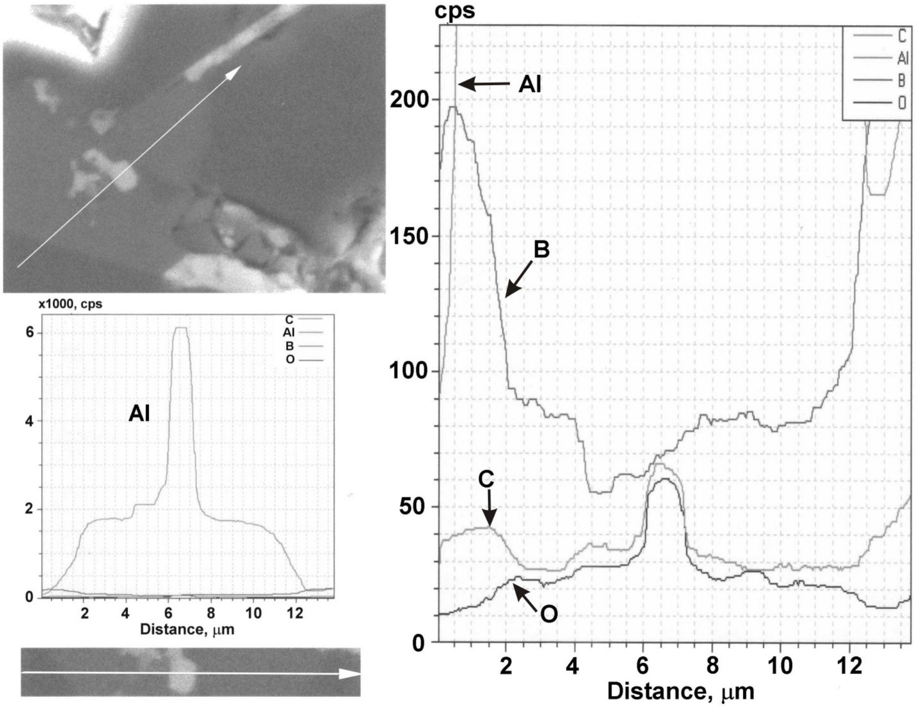

Figure 21. SEM-EDS line scan of an interfacial zone

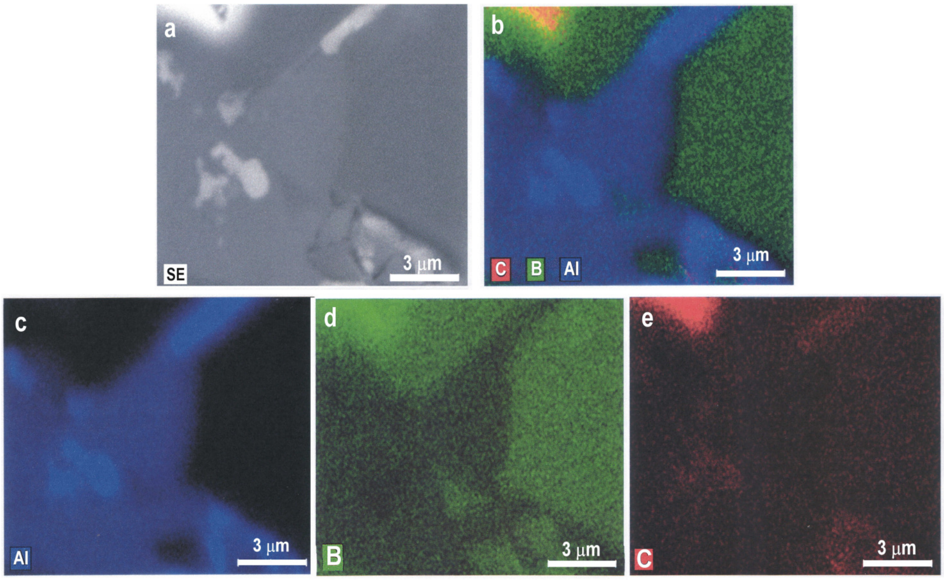

Figure 22. SEM-image of an interfacial zone (a) with mapping showing overall (b) and individual distribution of Al (c), B (d) and C (e); the lighter area in c, d and e indicates higher content

The analysis of the interfacial zone along with the XRD results (Fig. 15) suggests that the phase formed at the interface of the present system is Al_3BC and the mechanism of its formation is similar to that described by Viala *et al.* [15]. An example of phase distribution and bridging of boron carbide by Al_3BC is shown in Fig. 23.

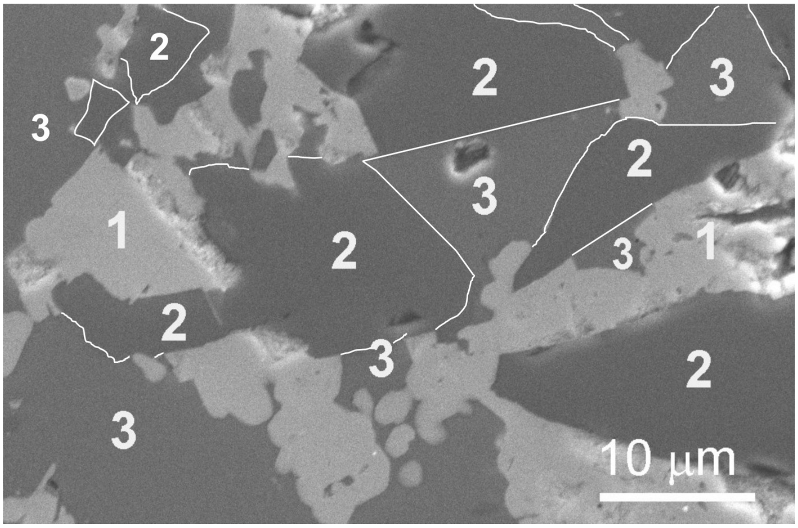

Figure 23. Phase distribution in B_4C-Al composite (grade C1080A): 1 – Al, 2 – B_4C, 3 – Al_3BC; white lines overlap some B_4C-Al_3BC interfaces

3.1.5 Concluding remarks

In general, it may be suggested that heat treatment is a tool for microstructure tailoring of as-synthesized composites. The combination of temperature and atmosphere allows one to modify the final microstructure of the composite in a desired way. As a result, different types of a microstructure can be developed (see Fig. 24): a particulate reinforced metal-matrix type (grade C0V and C700V), an interpenetrating co-continuous type (C1080V, C1150V, C1080A and C1470A), and a ceramic-matrix type with isolated binder islands (C1300V and C1500V).

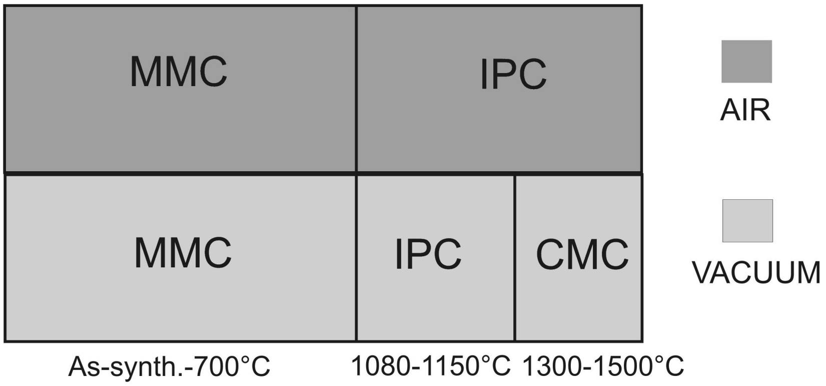

Figure 24. Microstructure types for B_4C-Al tailorable through heat treatment

The microstructural transformations are possible as long as a residual metal is present. The composites vary in their densities (between 2.13-2.60 g/cm^3), contiguity of ceramic phases and degree of interpenetration. The degradation of the microstructure in the form of voids generation is the main disadvantage of heat treatment in vacuum. This is because of high reactivity between initial components at high temperatures in vacuum accompanied with the formation of phases with higher densities and depletion of aluminum. Reactivity is suppressed when air is used as a processing environment.

The reaction products were determined using XRD. The formation of high-temperature phases (Al_4C_3, Al_3BC_3) was found to be significantly suppressed when air is used as processing environment instead of a vacuum. As distinct from [15, 24, 25] no AlB_2 was formed as a result of heat treatment at temperatures below 1000 °C and no high-temperature phases such as $AlB_{24}C_4$ and AlB_{12}.

XRD along with quantitative microstructural analysis suggest that heat treatment in air provides higher residual metal content.

The mechanism of B_4C-Al interfacial reaction resulted in the formation of ternary carbide Al_3BC as a main reaction product was found to be similar to that described by Viala *et al.* [15], i.e. in the beginning Al saturates in B and C near the interface, then Al_3BC nucleates and grows by the dissolution and the passivation of B_4C. The crystals of Al_3BC join together and form a quasi-continuous network changing the type of the microstructure.

3.2 Mechanical characterization

3.2.1 Indentation response

Response to indentation for the materials of interest was characterized by means of the microhardness of phases, conventional Vickers hardness, and instrumented indentation, also known as depth-sensing indentation, which, in fact, provides additional data allowing one to evaluate other properties including the elastic modulus.

Fig. 25 shows the average values for Vickers microhardness of phases presented in Figs. 11 and 12.

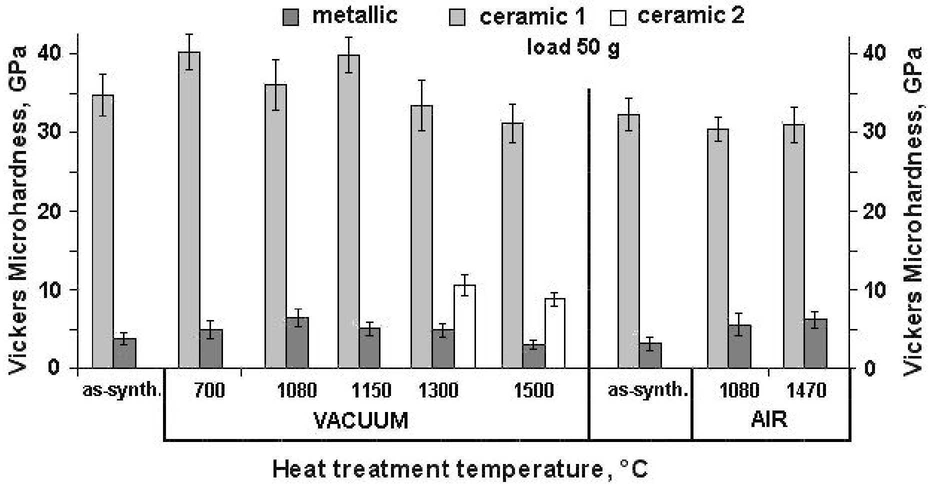

Figure 25. Vickers microhardness for phases of B_4C-Al (see Figs. 11 and 12)

Intensification of B_4C passivation and dissolution with the heat treatment temperature results in lowering the hardness of the mean ceramic phase (referred to as ceramic 1 in Fig. 25). At the same time the microhardness of metallic phase tend to increase due to nucleation and growth of reaction products. The values of microhardness are believed to be influenced by the arrangement and connectivity degree of phases. The continuous ceramic phase is expected to have higher hardness than that of a particulate surrounded by a soft metallic matrix. Based on the results of XRD (see Fig. 14), the phase referred to as ceramic 2 with the microhardness of 960-1100 HV0.05 is aluminium diboride AlB_2.

Table 7 summarizes the results of Vickers hardness (HV) measurement along with Martens (HM) (previously referred to as universal hardness) and indentation hardness (H_{IT}) obtained using instrumented indentation. The elastic modulus *E* for materials was evaluated from the unloading part of the load-indentation depth curve using the Oliver-Pharr approach [62].

Table 7. HV, HM, H_{IT}, and *E* values for B_4C-Al

Grade	HV10		HM, MPa		H_{IT}, MPa		*E*, GPa		
	Mean	PCV, %	Mean	PCV, %	Mean	PCV, %	Mean	PCV, %	
C0V	198	4.6	1684	5.2	1975	8.0	88	5.4	
C700V	279	5.2	2048	7.8	2559	9.1	93	7.0	VACUUM
C1080V	465	8.0	3324	5.6	4553	11.2	131	8.9	
C1150V	487	6.3	3447	6.3	4625	13.8	143	8.4	
C1300V	338	9.8	2243	8.9	2660	8.8	117	16.6	
C1500V	346	11.3	2498	10.2	3075	11.0	133	12.2	
C1080A	809	5.6	5562	7.1	8293	10.8	213	20.1	AIR
C1470A	450	7.1	3306	8.1	4343	6.5	153	11.2	
F1080A	501	6.2	3489	12.9	5124	14.1	123	10.0	
F1470A	463	7.7	2926	6.0	4082	5.0	135	8.5	

PCV – percent coefficient of variation

Changes in hardness and modulus would be strongly affected by microstructural transformations. The indentation loads used were sufficient to produce impressions over a number of grains. The number of bulk hardness of porous materials is referred to as an apparent value of hardness and is underestimated, since the result is influenced by the compression of sample imperfections along with the material. Thus, the value of true bulk hardness is influenced by the porosity, microhardness of individual grains, i.e. by the crystal structure of grains, and by orientational relationship between the grains. The values of Vickers hardness obtained for grades C0V and C1080A (porosity 2-4%) are accepted to be 'near-true' bulk hardness.

The hardness values for the composites of the B_4C-Al system obtained by other methods vary significantly: Levin *et al.* [37] have reported 500-2500 HV2, Jung and Kang [64] – 1100 HV20, Abenojar *et al.* [98] – 70-220 HV30. In all cases the initial content of boron carbide was at least 50 wt.%. Elastic modulus for B_4C-Al composites with ceramic content was reported by Miserez *et al.* [99] – 169 GPa.

3.2.2 Bending response

The three-point flexural strength of the B_4C-Al composites depending on processing conditions and microstructural characteristics is shown in Fig. 26.

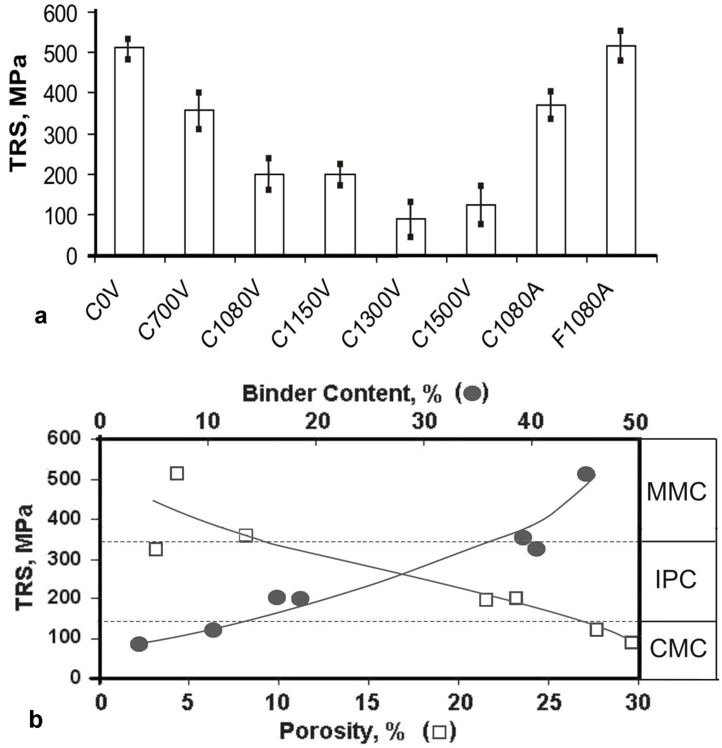

Figure 26. Transverse rupture strength (TRS) values for B_4C-Al composites

Strength was found to vary between 89 and 513 MPa for coarse-grained composites. Large scatters were found for grades C1300V and C1500V. The change in the bending strength is related to the changes in microstructure. There is a significant drop in the bending strength with an increase in the temperature of vacuum heat treatment. Voids generation, decreasing content of the ductile binder and formation of hard brittle reaction products are the determining factors. When comparing the TRS values for grades C1080V and C1080A, porosity is accepted to be of the highest influence. This is in agreement with the Griffith's theory of fracture quoting the initiation of brittle matrial failure as a result of tensile stresses at the tips of microstructural imperfections [100]. When comparing the TRS values for C0V and C1080A, which have quite equal volume fraction of porosity, it is assumed that strength reduction is also due to the formation of reaction products and the depletion of the binder. Surely, another contributing factor is the variety of phases. Large numbers of reaction products cause inhomogeneities in the material and reduce its strength. Thus, vacuum heat treatment at temperatures above 1000 °C significantly reduces the strength.

It is difficult to determine the effect of the contiguity of ceramic phases and interpenetrating nature on the bending strength, because other microstructural parameters are variable. Pyzik and Beaman [25] have found the flexural strength of B_4C-Al with the connected B_4C structure higher than that of the composites with an isolated B_4C. In the present study the composites with a continuous ceramic structure (IPC-area, Fig. 26b) experienced lower bending strength than those with the discontinuous boron carbide phase (MMC-area, Fig. 26b).

The B_4C-Al-cermet manufactured from fine-grained boron carbide B_4C powder showed higher TRS values than those manufactured from coarse-grained B_4C-powder. The reasons of this strengthening have not been explained because no adequate microstructural analysis for fine-grained composites is available. But it is known that in general higher densities, grain refinement, reduction of porosity are accepted to be the direct consequence of improved strength [101].

The bending strength of the boron carbide-aluminum composites derived by the exothermic reaction and subsequent heat treatment was found to match the strength of B_4C-Al composites with high ceramic content (at least 50 wt.%), which were obtained by other methods: 280-550 MPa [25], 300-700 MPa [37], 355-460 MPa (4-point bending) [102], 100-260 MPa [98].

3.2.3 Fractography

SEM observations of the fractured surfaces suggest different failure behavior of the samples processed at different conditions. Fig. 27 represents a general view of fracture surface of selected grades heat-treated in vacuum at different temperatures. Fractography also provides additional insight into the development of a continuous ceramic skeleton and open porosity (Fig. 27d).

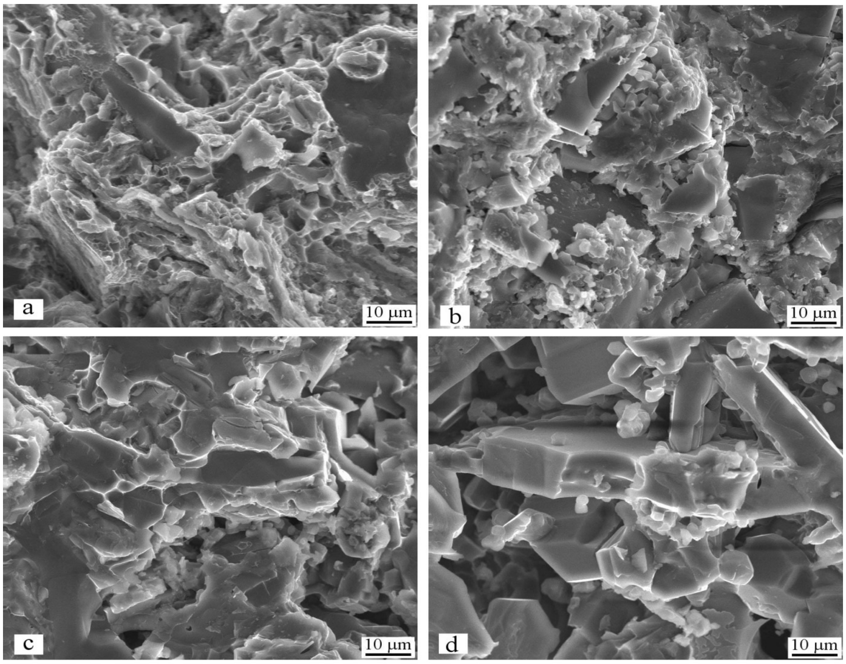

Figure 27. Fracture surfaces: a - grade C0V, b - C1080V, c - C1150V, and d - C1500V

Fractography shows a rough and irregular dimpled fracture surface for an as-synthesized material, indicating ductile fracture. Interface rupture at B_4C grains and non-planar crack front in grade C0V suggest that the interface is the weakest link and an insufficient bonding. The ratio between brittle transgranular cleavage and ductile dimple fracture becomes significantly higher with the heat treatment temperature increasing. Grade C1500V failed by pure transgranular cleavage.

The fracture surface of sample C1080A showed in Fig. 28 appears to be composed of two differently behaved zones: highly-reacted and poorly reacted.

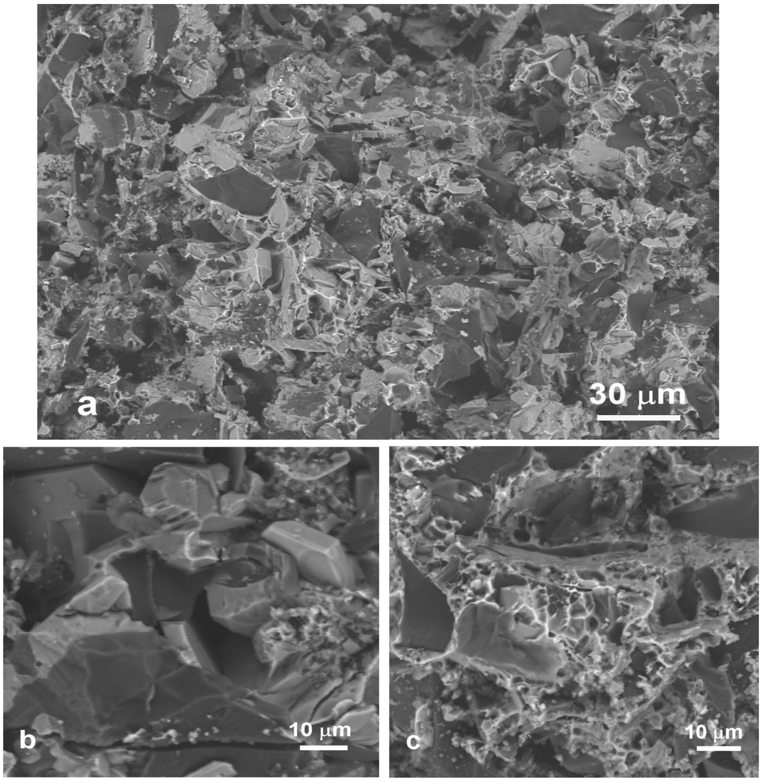

Figure 28. Fracture surface of grade C1080A: a – general view, b – highly-reacted zone, c – poorly-reacted zone

The highly-reacted zone of the fracture surface is strongly cleavaged with some brittle striations, while the poorly-reacted is dimpled.

3.2.4 Concluding remarks

Changes in the microhardness of the phases are related to microstructural transformations. Decreases in microhardness of the main ceramic phase are explained by the passivation of boron carbide and the formation of reaction products of lower hardness.

The bulk hardness measured for B_4C-Al composites is referred to as apparent hardness due to the high volume of voids. The near-true values of bulk hardness and reduced elastic modulus are believed to have been estimated for grades C0V and C1080A, which have a relatively low porosity.

Porosity and residual metal content are the main parameters that determine the flexural strength. The highest strength was shown by the composites of the MMC-type structure, while the lowest – the composites of the CMC-type structure.

Fractography showed transition from ductile to brittle fracture with an increase of the heat-treatment temperature. Fig. 27d indicates open porosity for grade heat-treated in vacuum at 1500 °C.

3.3 Dry sliding wear

3.3.1 Wear quantification

The variation of the volumetric wear *W* with sliding distance *L* under three different normal loads *F* for the composites synthesized from the coarse-grained B_4C powder is shown in Fig. 29.

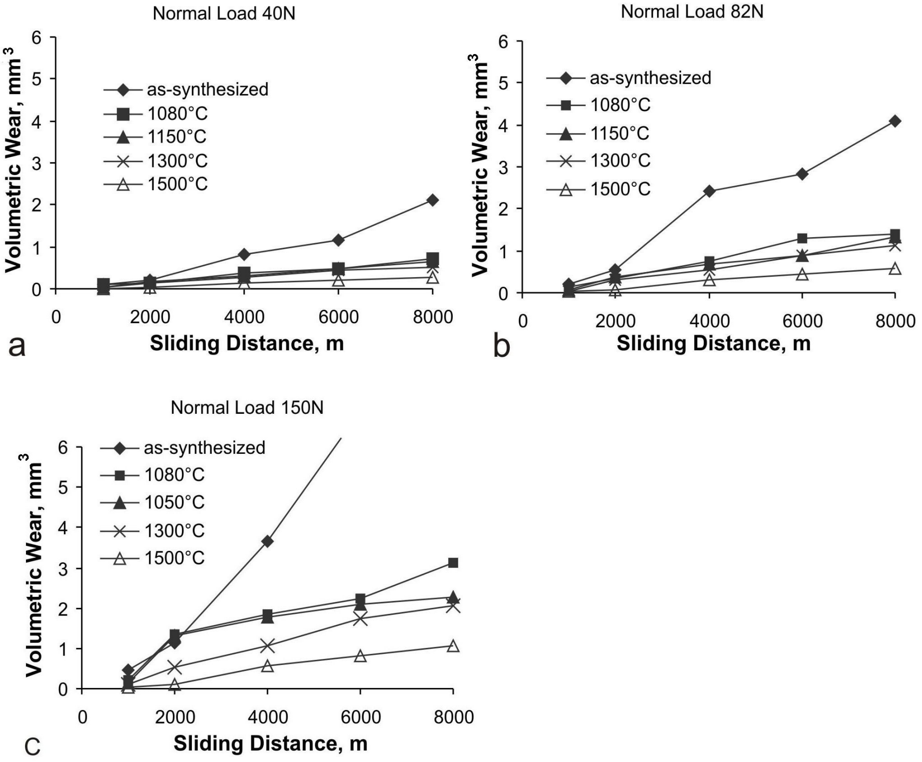

Figure 29. Volumetric wear *vs.* sliding distance for coarse-grained B_4C-Al composites at normal loads of: a – 40 N, b – 82 N, c – 150 N (sliding velocity 2.2 m/s)

The highest loss is demonstrated by the as-synthesized material (grade C0V). The samples subjected to the secondary thermal processing experienced a lower wear, while the increase in the temperature of heat treatment results in a wear decrease.

Plots in Fig. 29c suggest a different evolution of the volumetric wear with sliding distance for the composites subjected to different heat treatment. For grades C1080V and C1150V the proportionality is initially curvilinear, representing the transient wear. Visual inspecting of the curves suggests that the end of transient wear is after about 2000 m of the sliding distance. During the steady-state there is a near-linear dependence between the volumetric wear and the sliding distance. For grades C1300V and C1500V the volumetric wear/sliding distance behavior is near-linear over the whole distance, i.e. there is no classical running-in or transient wear over the observed distance.

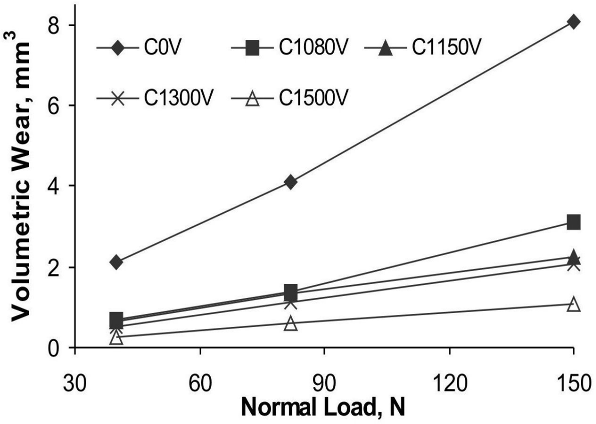

Figure 30. Variation of volumetric wear with normal load (8000 m, 2.2 m/s)

As it can be seen from Fig. 30, the volume of the material removed increases linearly with the normal load, indicating no transition load in the range of 40-150 N.

The influence of the conditions of heat treatment processing along with the effect of initial carbide grain size on the sliding wear resistance of B_4C-Al composites is presented below. Specific wear rate W_{sp}, i.e. volume loss per unit sliding distance per unit applied load was used to compare the wear resistance of the materials:

$$W_{sp} = \frac{W}{FL} \tag{6}$$

where W_{sp} – specific wear rate (mm^3/Nm), W – volume loss (mm^3), F – applied normal load (N), L – sliding distance (m).

The curves in Fig. 31a show variations of W_{sp} with L during the initial period of the test that can be explained by unstable friction during running-in period.

Fig. 31b represents the average specific wear rate values obtained over the whole distance and over the steady-state regime.

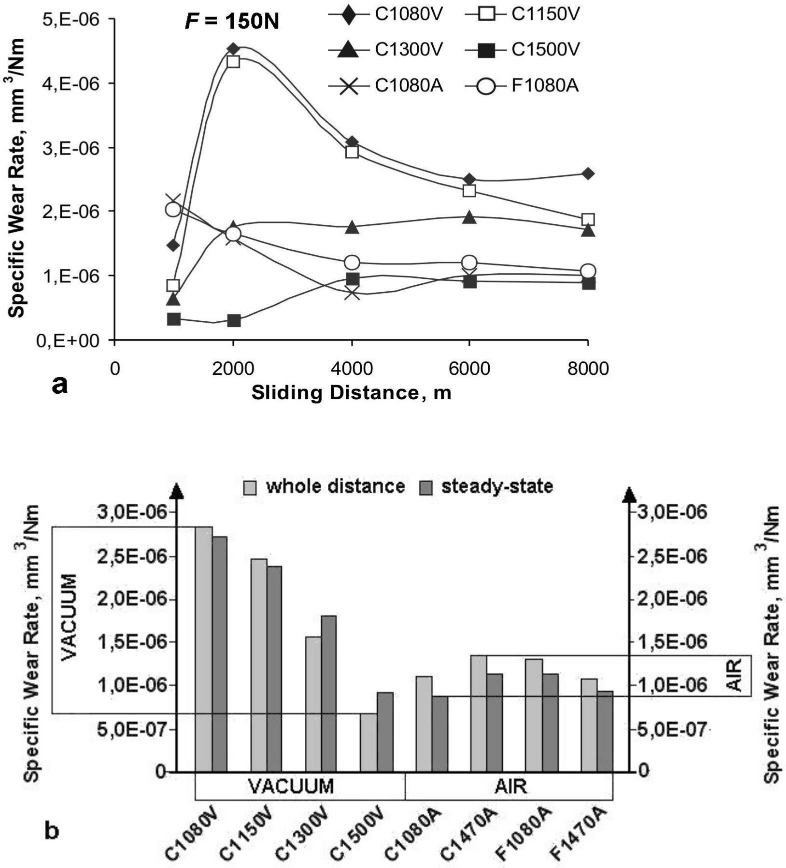

Figure 31. Specific wear rate for B_4C-Al: a – variation with sliding distance at normal load of 150 N; b – average values for heat-treated grades obtained under normal loads of 40, 82 and 150 N

Table 8 shows the percent coefficient of variation for specific wear rate W_{sp} data represented in Fig. 31b.

Table 8. Percent coefficient of variation of specific wear rate W_{sp}

	COV	C1080V	C1150V	C1300V	C1500V	C1080A	C1470A	F1080A	F1470A
wd, %	36.5	39.5	52.6	33.4	48.2	39.9	25.5	23.2	20.8
ss, %	11.6	11.3	22.2	5.9	4.4	12.7	7.7	8.6	5.7

wd – whole distance, ss – steady-state regime

The values of the specific wear rate for all samples are in the order of 10^{-6} mm^3/Nm, which suggests a high wear resistance under given conditions. There is an obvious decrease in the wear rate with an increase of heat treatment temperature for coarse-grained samples heat-treated in vacuum. This can be explained by the development of hard ceramic skeletal network as a result of heat treatment. Wear resistance enhancement can also be explained by the development of a continuous interpenetrating structure that appears to offer advantages over particulate structures [103-106].

Fig. 31a shows different behaviors of B_4C-Al composites during running-in. Grades of the CMC-structure with a low content of metallic phase (C1300V and C1500V) have the lowest wear rate during the running-in. In contrast, grades with a continuous metal phase of higher content are subjected to the highest wear at the initial stage that tends to decrease and stabilize.

Testing showed no significant differences between wear rate values for samples heat-treated in air at temperatures of 1080 °C and 1470 °C (grades C1080A and C1470A), while the wear rate of the sample heat-treated in air at 1080 °C was lower than that of heat-treated in vacuum at the same temperature. The wear test results suggest also that there is no significant difference in wear rate of samples synthesized from coarse- and fine-grained B_4C powder. It can be concluded also that test runs shorter than 4000 m do not allow an adequate characterization of the steady-state wear behavior of B_4C-Al composites.

Comparative tests under the same conditions were performed with the blocks of WC-Co (15 wt.% Co) and TiC-NiMo composites (15 wt.% Ni, 15 wt.% Mo) having densities of 13.9 and 5.7 g/cm^3, respectively [107]. The results are presented in Table 9. Results for WC-Co and TiC-NiMo composites with a different binder content obtained under similar testing conditions have been reported by Pirso et al. [107, 108].

Table 9. Comparative W_{sp} values (percent coefficient of variation in parentheses)

	Experiment							Literature	
Material	C1080V	C1150V	C1500V	C1080A	F1080A	WC-Co	TiC-NiMo	WC-Co	TiC-NiMo
W_{sp} ×10^{-6} mm^3/Nm	2.83	2.46	0.69	1.11	1.31	0.46 (33.8%)	0.38 (19.8%)	0.43-0.86 [108]	0.35-1.25 [107]
Bulk Density, g/cm^3	2.3	2.4	2.1	2.6	2.5	13.9	5.7	13.5-14.8 [108]	5.5-6.5 [107]

As it can be seen from Table 9, wear rate values for selected B_4C-Al grades are somewhat higher, but comparable with those of WC-Co and TiC-NiMo. However, when the mass loss is taken into account, lightweight B_4C-Al composites have advantages over WC-Co and TiC-NiMo.

3.3.2 The role of mechanical properties

The results of wear experiments were analyzed in terms of mechanical properties derived from instrumented indentation and summarized in Table 10.

Table 10. Specific wear rate and parameters obtained by instrumented indentation

Grade	W_{sp} ×10^{-6}, mm^3/Nm	HM/*E*	H_{IT}/E	W_t, mJ	W_p, mJ	W_p/W_t	h_r, μm	W_t/h_r
C0V	6.8	0.019	0.022	1.510	1.422	0.942	41.02	36.81
C1150V	2.38	0.024	0.032	1.129	0.920	0.814	26.47	42.65
C1080A	0.86	0.026	0.039	0.855	0.524	0.634	17.22	49.65
C1470A	1.14	0.022	0.028	1.143	0.966	0.845	25.96	44.03
F1080A	1.14	0.028	0.042	1.045	0.798	0.764	23.97	43.60
F1470A	0.95	0.022	0.030	1.172	0.913	0.779	26.39	44.42

W_t – total indentation work, W_p – plastic indentation work, h_r – residual depth of indent

Hardness is usually considered as the most important mechanical property in the characterization and prediction of wear [90]. Indentation hardness H_{IT} is assumed to be close in value to the plastic flow stress for a material [68]. No correlation was found between apparent bulk hardness HM and H_{IT} and wear characteristics for B_4C-Al probably because of different void fraction of the composites. However, there is an obvious dependence between the volume wear and the volume fraction of ceramic phases. The microstructural development resulting in the transformation of the composite from a metal-matrix type into a ceramic-matrix type with a higher microhardness of the matrix leads to the improvement of wear resistance.

The ratio of hardness to the elastic modulus, which is another important parameter in tribology and fracture mechanics, showed also no correlation with the specific wear rate W_{sp}.

Parameter W_t/h_r was found to correlate with the specific wear rate W_{sp} values. Since h_r is the residual depth of indent, i.e. the total plastic deformation, the parameter W_t/h_r characterizes the ability of the material to withstand plastic deformation [109].

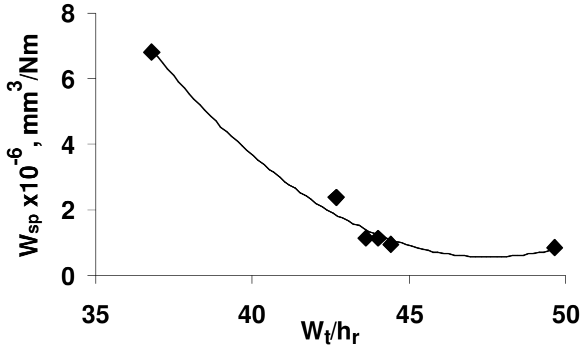

Figure 32. Dependence of specific wear rate W_{sp} with W_t/h_r

The correlation shown in Fig. 32 suggests that wear of B_4C-Al is related to plasticity under given operating conditions and it occurred below the Griffith criterion, i.e. the tensile stresses developed under given conditions in the wearing contact are lower than the critical fracture stress of B_4C-Al.

3.3.3 Friction coefficient and friction temperature

The friction tests produced friction coefficient values averaging between 0.35 and 0.45 for 150 N load, which remained constant throughout the test as the material wears and the friction temperature increases. The maximal fluctuations of the friction coefficient values have been observed during the running-in period (within the first 2000 m). Fig. 33 summarizes the average values of the coefficient of friction during the running-in and the steady-state friction for the selected grades.

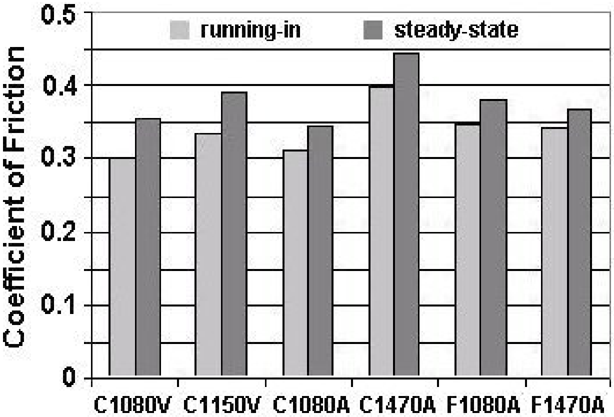

Figure 33. Average values of coefficient of friction during running-in and steady state; $F = 150$ N, $v = 2.2$ m/s, $L = 8000$ m

In general, the results showed that higher friction is experienced by the grades heat-treated at higher temperatures (consequently, having larger fraction of in-situ phases) among those fabricated from coarse B_4C.

No direct correlation between the microstructural characteristics and the frictional temperature was observed probably due to insufficiently precise measurement of the temperature. Fig. 34 shows an example of the coefficient of friction and the bulk frictional temperature profiles. Although there was no exact reproducibility of the friction coefficient and friction temperature curves, a general behavior is characterized by these plots. On average, the bulk frictional temperature of the contact surface varied between 80-100 °C and 170-200 °C at normal loads of 40 N and 150 N, respectively. An opposite surface here is the surface of the block that is opposite to the friction contact surface.

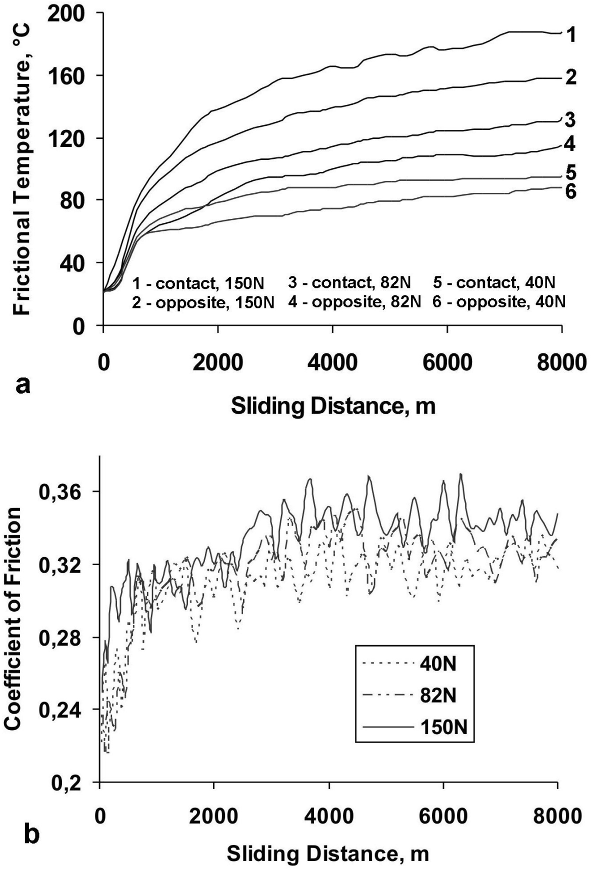

Figure 34. Characteristic profiles for bulk frictional temperature of contact and opposite surfaces (a) and coefficient of friction (b); grade C1080A

No general correlation between the specific wear rate and the coefficient of friction was found for the investigated materials. This inconsistency between friction and wear may be caused by the fact that any effects that friction may have on the wear rate, would not only be dependent on the magnitude of the load and the friction force, but also on the nature of the materials in contact [68].

3.3.4 Relationship between wear and dissipated energy

The wear of the materials was analyzed by means of the dissipated frictional energy E_d that was calculated as the work of the frictional force F_f according to Eq. (7) [110]:

$$E_d = F_f\, v\, t = \mu\, F\, v\, t \qquad (7)$$

where the v the relative sliding velocity (m/s), t the duration of sliding test (s), μ the coefficient of friction.

The product of the relative sliding velocity and the duration of the sliding test can be replaced with the sliding distance *L*. Frictional force is known to be the product of the normal load *F* and the coefficient of friction μ. The energetic approach of wear characterization takes into account the evolution of the friction coefficient, i.e. frictional force, thus providing an advantage to study the tribosystems with unstable friction [77]. The plots of the volumetric wear versus the dissipated energy are presented in Fig. 35.

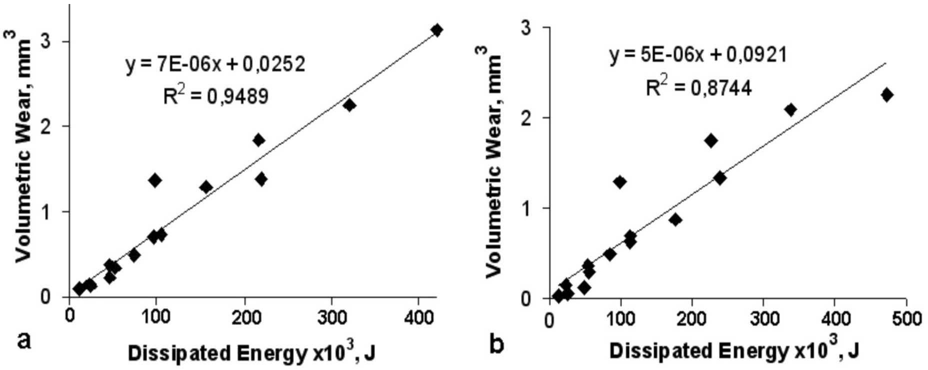

Figure 35. Variations of volumetric wear with dissipated frictional energy: a – C1080V, b – C1150V (normal load range 40-150 N, constant sliding velocity 2.2 m/s)

The preliminary results suggest a linear relation between the volumetric wear and the dissipated energy. This assumes no transition between mild and severe wear in a range of normal loads 40-150 N at a given linear speed. Surely, testing under a wider range of operating conditions including variable sliding velocity is needed to estimate the wear by means of the dissipated energy approach.

3.3.5 Worn surfaces and proposal for wear mechanisms

The blocks subjected to dry sliding were analyzed by OM and SEM. The worn surface of grade C0V after 1000 m of sliding is shown in Fig. 36, indicating grain pullouts (areas of black color).

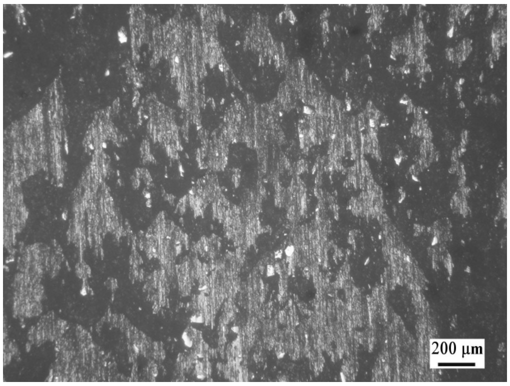

Figure 36. OM-micrograph of C0V worn surface after 1000 m of sliding at 150 N

The wear of the as-synthesized material occurred by the ejection (extrusion) of a soft binder and pullout of B_4C grains no more supported by the removed binder. B_4C grains act as abrasive particles when trapped into the frictional interface (see Fig. 5a) and cause many deep parallel grooves.

Fig. 37 shows the worn surfaces of selected vacuum heat-treated grades after 1000 and 8000 m of sliding at normal load of 150 N.

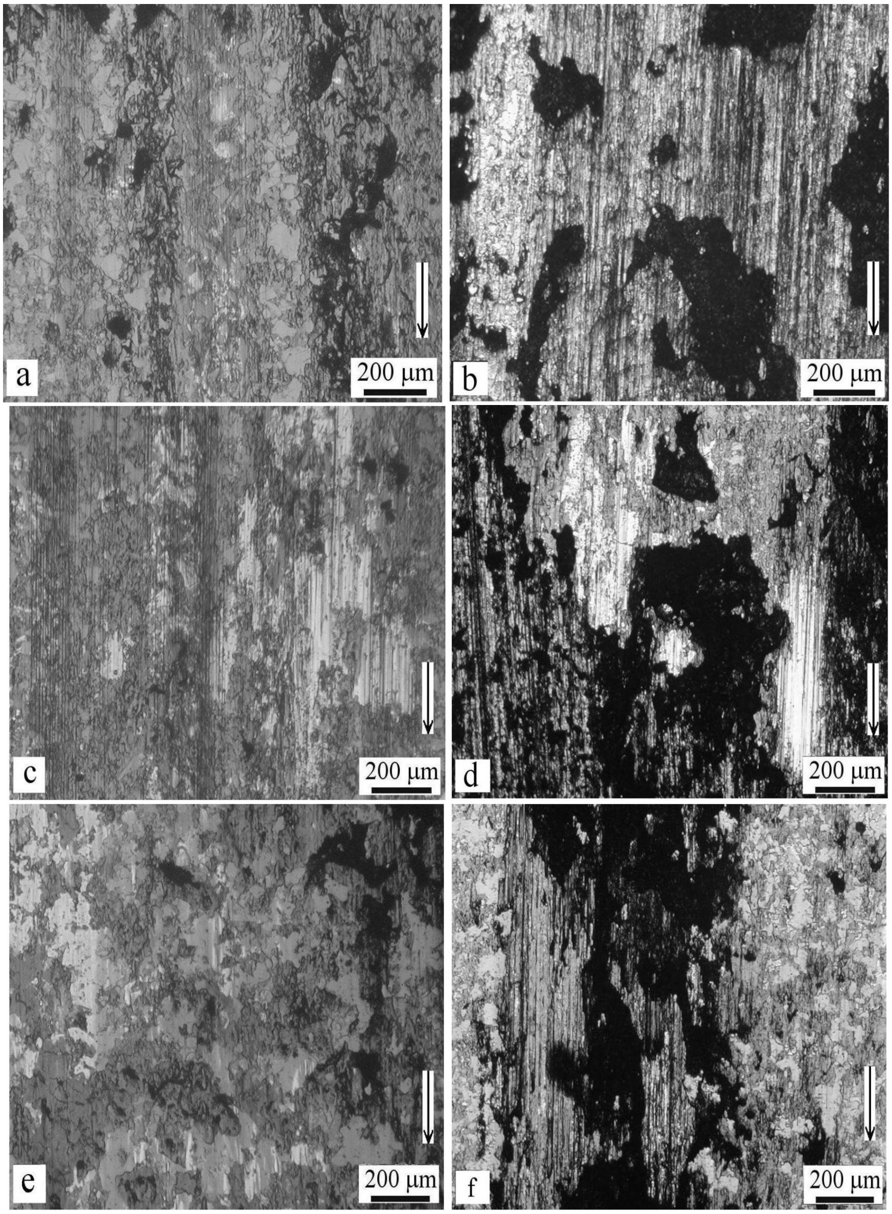

Figure 37. Optical micrographs of worn surfaces: grade C1080V (a – 1000 m, b – 8000 m), grade C1150V (c – 1000 m, d – 8000 m), grade C1500V (e – 1000 m, f – 8000 m). Arrows show sliding direction, load 150 N

Two different zones can be explored on the worn surfaces: rough zones indicating severe wear and smooth luster zones. The worn surfaces in Fig. 37 were found to be similar in appearance between grades, thus indicating a similar wear mechanism distinct from that of grade C0V. The formation of glaze was observed after the very first kilometer of sliding, and the worn surface represents a combination of islands of a tribofilm with islands of a bare microstructure. No significant grain pullout was observed after 1000 m. After 8000 m of sliding the worn surfaces were observed to change remarkably. They became rougher and had large areas of black color areas as a result of tribofilm removal and grain pullouts; there were grooves and some surface cracks visible also.

Fig. 38 represents the worn surfaces of grade C1080A after 1000 and 8000 m of sliding at normal loads of 40 and 150 N.

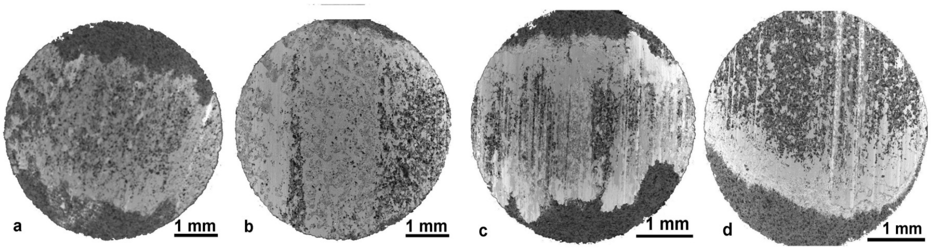

Figure 38. Worn surfaces of C1080A: a – 40 N, 1000 m; b – 40 N, 8000 m; c – 150 N, 1000 m; d – 150 N, 8000 m

At a normal load of 40 N the worn surface is uniformly coated with a tribofilm (Fig. 38a and b), while at the load of 150 N the bare structure is visible in the central zone of wear track, especially after longer runs (Fig. 38c and d). This implies a higher rate of tribofilm removal at heavier loadings.

A detailed characterization of transfer layers was performed by means of SEM and XRD. SEM elemental maps confirmed the presence of iron and/or Fe containing compounds on the worn surfaces of all the blocks (see Fig. 39), while XRD showed reflections from Fe_2O_3 instead of Fe. These investigations revealed disk material transfer and its oxidation.

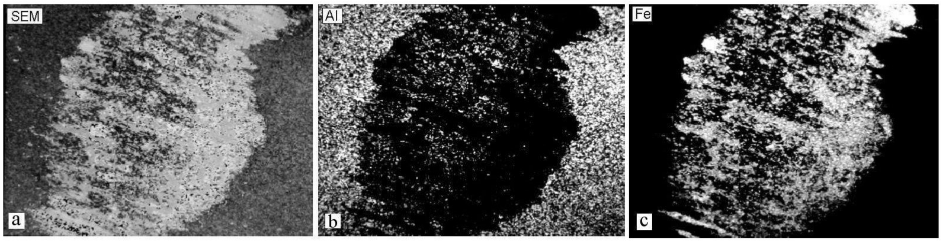

Figure 39. SEM elemental map of worn surface (grade C1080V, 150N, 2000 m)

Iron oxides are known to act as lubricants and therefore improve the wear resistance and provide smooth friction [111]. Moisture in the surrounding air along with the frictional temperature accelerates the oxidation of the transferred material.

A characteristic view of different zones of a tribofilm is shown in Fig. 40.

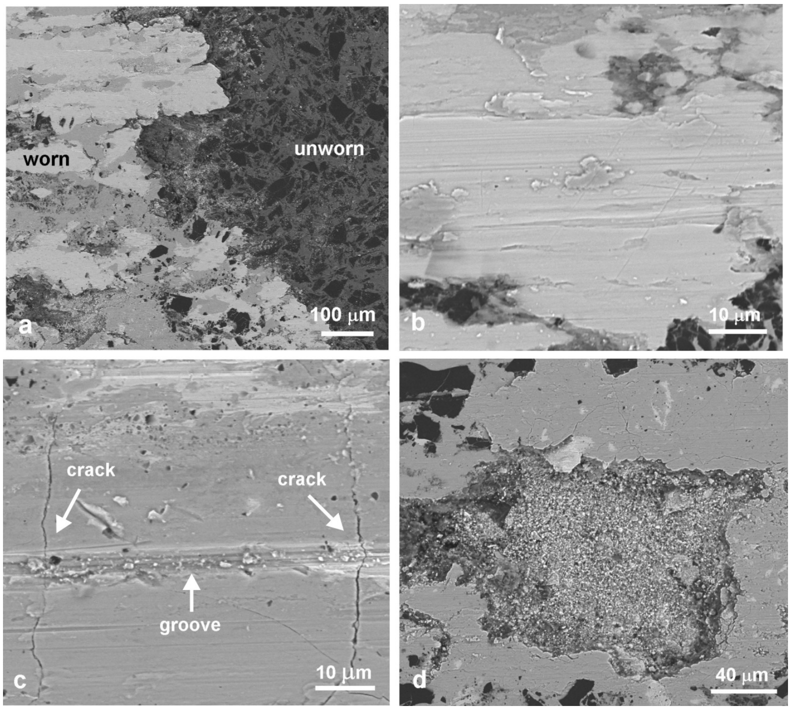

Figure 40. SEM-micrographs showing worn and unworn areas of surface (a), smearing of transfer features (b), area of highly compacted cracked tribofilm (c), pit formed by tribofilm removal (d); load 82 N, distance 2000 m

Tribofilms were observed to be smooth except a few deep grooves (Fig. 40c), whereas film removal occurred by fracturing. The grooves revealed ploughing caused by hard debris particles moving across the interface. The hard particles may be trapped into the interface when the grains of B_4C and/or reaction products are no more supported by the binder torn away or when they are cracked and fragmentized. Load carrying ridges smeared in the sliding direction are seen in Fig. 40b. The cracks in tribofilm normal to sliding direction (Fig. 40c) are typical cracks developed by tension during ploughing. In such a case extreme levels of local plastic deformations along with the internal tensions caused by the frictional temperature gradient are responsible for surface and sub-surface cracks [70, 107]. When the cracks become connected, a piece of material is detached and a pit in the surface is present. A network of microcracks in the transferred layer is observed around the pits formed as a result of film spalling. The bared surface is protected from wear and smearing as long as it remains below the contact surface level. Yao *et al.* [111] have shown the possibility of regeneration of a worn surface by filling of the pits with the wear debris welded together.

Wear quantification and characterization of worn surfaces reveal similar wear mechanisms for secondary processed B_4C-Al and the occurrence of several basic processes during sliding: transfer (adhesion), interactions with the environment (oxidation), tribofilm deformation (plastic flow), mechanical mixing, and fracture. The occurrence of low wear is proposed to be a direct inference of the formation of oxide containing layer. However, differences in the specific wear rate suggest that the extent and intensity of each particulate process vary with B_4C-Al grades.

The wear of B_4C-Al is an equilibrium process of tribofilm formation, tribofilm removal and the wear of a bare structure. A tribofilm is formed as a result of material transfer, mixing, smearing and oxidation. The smeared layer is then subjected to plastic flow and at a certain stress it is removed by delamination and/or microfracture. The shear stress developed at the tribofilm/base material interface or within the layer itself determines the rate of tribofilm removal. Voids may play an important role in microcracking and fracture, since they are potential sources for crack origination due to deformation and stress increase. However, no increase in wear with porosity was observed under given testing conditions for vacuum heat-treated grades, suggesting that stresses developed as a result of indicated testing conditions were not high enough to cause the fracture from pre-existing flaws. A bare structure is involved in the wear as long it remains unprotected by the regenerated tribofilm.

3.3.6 Wear rate prediction

The volume of the material removed by wear was predicted using the exponential and Yang's model described in Section 2.2.3. Wear tests for the grades C0V, C1080V, C1150V, C1300V and C1500V were carried out at normal loads of 40, 82 and 150 N, over sliding distances of 1000, 2000, 4000, 6000 and 8000 m, and at a constant linear sliding speed of 2.2 m/s.

Experimental and predicted volumetric wear values for B_4C-Al composites under different normal loads are shown in Fig. 41.

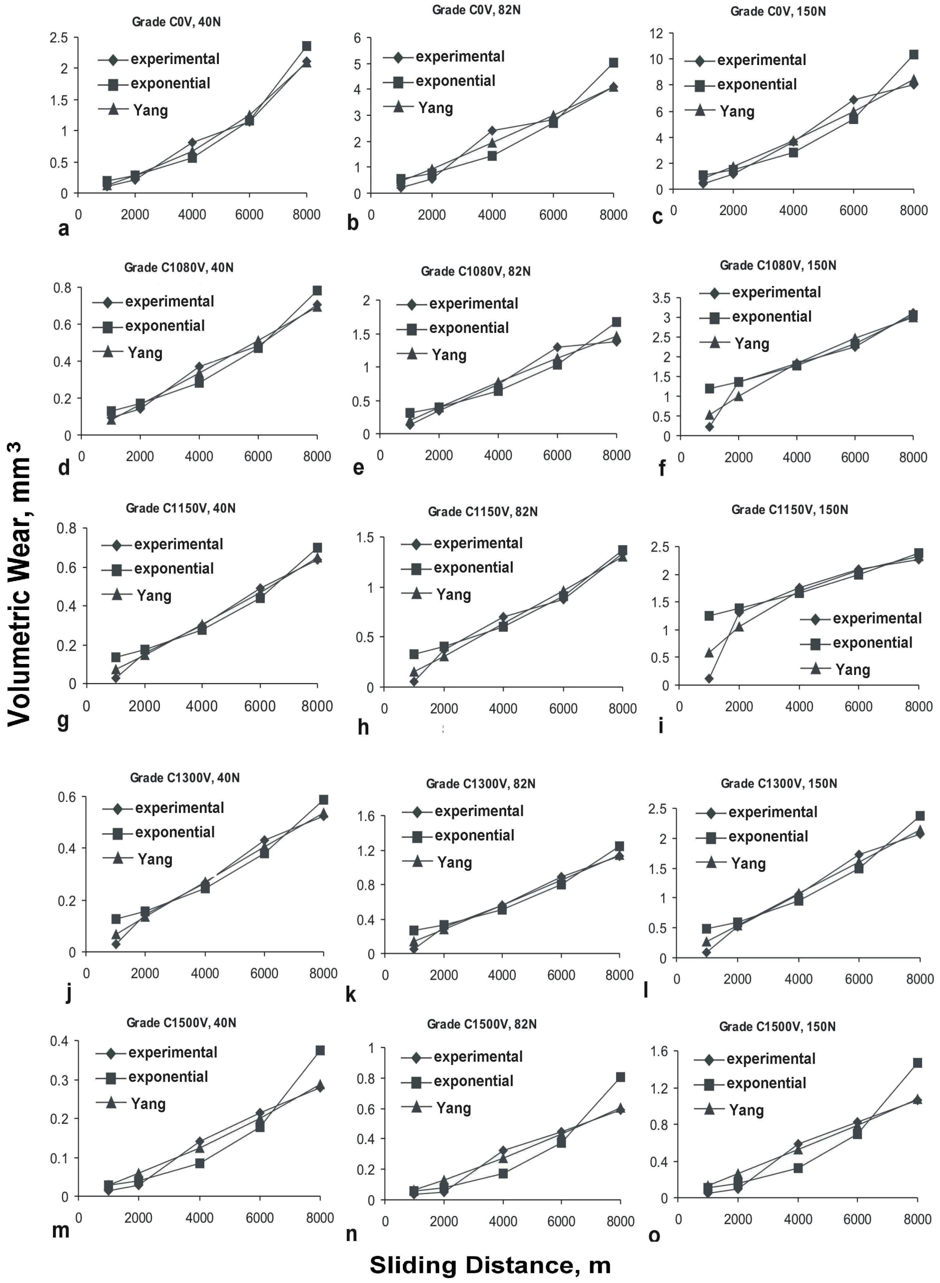

Figure 41. Experimental and predicted wear volume

The accuracy of wear volume prediction was characterized by the percentage deviation ΔW calculated accordingly to Eqs. (8) and (9).

$$\Delta W_E = \left(\frac{|W_E - W|}{W_{\exp}}\right) \times 100\% \tag{8}$$

$$\Delta W_Y = \left(\frac{|W_Y - W|}{W_{\exp}}\right) \times 100\% \qquad (9)$$

where ΔW_E and ΔW_Y – percentage deviations of volumetric wear predicted by exponential and Yang's model, respectively; W – experimental volumetric wear; W_E and W_Y – volumetric wear predicted by exponential and Yang's model, respectively.

Table 11 shows the percentage deviations of predicted volumetric wear values against experimental ones.

Table 11. Deviations of predicted wear volume against experimental

GRADE C0V														
F, N	ΔW_E, %							ΔW_Y, %						
	Sliding distance $L \times 10^3$, m					Average*		Sliding distance $L \times 10^3$, m					Average*	
	1	2	4	6	8	wd	ss	1	2	4	6	8	wd	ss
40	80.7	26.4	29.8	0.7	12.1	29.9	14.2	16.0	25.1	16.7	8.7	1.2	13.5	8.8
82	181.2	43.6	40.4	5.2	22.9	58.7	22.8	128.0	73.1	20.6	4.9	0.3	45.4	8.6
150	137.3	29.1	22.9	21.7	22.9	46.8	22.5	93.8	56.6	3.2	13.1	0.3	33.4	5.5
GRADE C1080V														
F, N	ΔW_E, %							ΔW_Y, %						
	Sliding distance $L \times 10^3$, m					Average*		Sliding distance $L \times 10^3$, m					Average*	
	1	2	4	6	8	wd	ss	1	2	4	6	8	wd	ss
40	41.9	20.4	23.3	2.4	11.1	19.8	12.3	12.4	16.3	9.3	6.1	1.3	9.1	5.6
82	142.0	17.4	12.2	19.5	20.8	42.4	17.5	54.8	16.6	5.3	12.5	5.6	19.0	7.8
150	444.3	0.5	2.9	4.3	20.8	94.6	9.3	142.7	25.7	1.0	10.4	5.6	37.1	5.7
GRADE C1150V														
F, N	ΔW_E, %							ΔW_Y, %						
	Sliding distance $L \times 10^3$, m					Average*		Sliding distance $L \times 10^3$, m					Average*	
	1	2	4	6	8	wd	ss	1	2	4	6	8	wd	ss
40	379.9	9.1	7.6	10.1	10.1	83.3	9.2	153.8	7.2	1.7	3.9	1.5	33.6	2.4
82	506.5	8.6	13.0	3.2	2.5	106.8	6.3	185.8	15.9	9.0	9.3	2.2	44.5	6.8
150	898.6	6.0	6.0	5.1	2.5	183.6	4.5	368.5	19.2	4.0	0.7	2.2	78.9	2.3
GRADE C1300V														
F, N	ΔW_E, %							ΔW_Y, %						
	Sliding distance $L \times 10^3$, m					Average*		Sliding distance $L \times 10^3$, m					Average*	
	1	2	4	6	8	wd	ss	1	2	4	6	8	wd	ss
40	353.1	10.3	7.8	12.2	12.1	79.1	10.7	145.0	4.5	2.4	6.1	2.5	32.1	3.7
82	422.7	9.5	7.9	10.4	10.5	92.2	9.6	176.1	7.0	1.3	4.4	1.8	38.1	2.5
150	396.7	13.1	10.6	13.5	10.5	88.9	11.5	180.4	1.5	1.2	7.4	1.8	38.4	3.5
GRADE C1500V														
F, N	ΔW_E, %							ΔW_Y, %						
	Sliding distance $L \times 10^3$, m					Average*		Sliding distance $L \times 10^3$, m					Average*	
	1	2	4	6	8	wd	ss	1	2	4	6	8	wd	ss
40	112.3	48.7	39.6	16.5	33.5	50.1	29.9	111.7	112.2	11.7	6.0	3.0	48.9	6.9
82	61.8	58.6	45.7	15.2	36.7	43.6	32.5	80.4	148.1	16.2	3.3	2.6	50.1	7.4
150	113.3	57.0	44.4	16.5	36.7	53.6	32.5	160.5	164.9	10.5	3.9	2.6	68.5	5.6

*average deviation: wd – whole distance; ss – steady-state distance (assumed to start at 4000 m)

It can be seen from Table 11 that in general Yang's model gives a more accurate prediction than that of the exponential model. It should be noted that neither of the models gives an adequate prediction for the running-in period, and in a majority of cases the predicted values are higher than experimental. Yang's model was originally proposed to predict the steady-state wear of Al-MMC with the transient wear data only. Deviation values for distances of 1000 and 2000 m have shown that such an approach cannot be used for the materials used in the current research. However, with sliding distances of 4000, 6000 and 8000 m, i.e. in the steady-state regime, Yang's model gives a good prediction (average deviations below 10 %) for the wear volume for all the grades investigated.

3.3.7 Concluding remarks

B_4C-Al composites showed high wear resistance comparable with that of WC- and TiC-based hardmetals and cermets under indicated operating conditions against carbon steel. No transition from mild to severe wear was observed in a range of normal loads 40-150 N at a constant linear velocity of 2.2 m/s.

It was observed that the specific wear rate is related to the quantity of the ratio of the total indentation work to the residual indentation depth. This parameter characterizes the ability to resist the plastic deformation. Thus, the correlation suggests that the wear of B_4C-Al is related to plasticity under given testing conditions and deformation caused during sliding does not lead to fracture.

The formation of the protective tribolayer containing Fe_2O_3 was found to be responsible for high wear resistance, irrespective of the secondary phases.

A model proposed by Yang [91] for wear prediction was found to give accurate results for the steady-state friction of B_4C-Al composites.

CONCLUSIONS AND SUGGESTIONS

Conclusions

1. The microstructure and properties of lightweight boron carbide-aluminum composites synthesized by the exothermic reaction can be tailored over a broad range to improve the wear resistance and match the strength of B_4C-Al materials obtained by other methods. The bulk density of the derived composites has been found to vary in a range of 2.1-2.6 g/cm^3 depending on the processing conditions. Depletion of aluminum due to formation of new phases and evaporation/outflow leads to the formation of pores and voids. The composites comprised at least one in-situ formed ceramic phase. In following the conditions of secondary processing for synthesized compacts are proposed to produce:
    - MMC-type composite with a bulk density of 2.4 g/cm^3 with a trace amount of only reaction product Al_3BC – vacuum heat treatment at 700 °C
    - co-continuous interpenetrating phase composite (bulk density 2.3-2.4 g/cm^3) with reaction products Al_3BC and a trace amount of Al_4C_3 – vacuum heat treatment at 1080-1150 °C
    - CMC-type composite (bulk density 2.1 g/cm^3) with reaction products Al_3BC, Al_4C_3, Al_3BC_3, and trace amount of AlB_2 – vacuum heat treatment at 1300-1500 °C
    - Co-continuous ceramic-metal composite with a bulk density of 2.6 g/cm^3 composed of Al, B_4C and Al_3BC – heat treatment in air at 1080 °C
    - Co-continuous ceramic-metal composite with a bulk density of 2.4 g/cm^3 composed of Al, B_4C, Al_3BC and Al_4C_3 – heat treatment in air at 1470 °C
2. The microstructure of the final composite was found to be sensitive to the processing environment. The extent of formation of main reaction product Al_3BC determines the structure type (MMC, IPC or CMC) and the property of final composite. Formation of the detrimental Al_4C_3 and other high-temperature phases will be avoided if heat treatment is performed at temperatures below 1100 °C.
3. In spite of microstructural defects (voids, pores) the material is capable to withstand the dry sliding wear against carbon steel under investigated conditions. The specific wear rate was found to be in the order 10^{-6} mm^3/Nm independent of the processing conditions. The high wear-resistance of B_4C-Al composites was found to be a direct inference of iron oxide containing transfer layers on the contact surface.

    Composites with MMC structure have the lowest wear resistance, but the highest flexural strength, thus they can be used in dry sliding conditions with dynamic loading. Composites with the CMC structure have higher wear resistance, but the lowest flexural strength. Dense B_4C-Al composites with the IPC structure have a better combination of strength and wear resistance.

   No significant influence of B_4C powder grain size was found on the wear resistance.

   The composites demonstrated a stabile coefficient of friction in the range of 0.35-0.45 and no fade with an increase in the bulk frictional temperature up to 200 °C.

   The volume of the material removed by wear during the steady-state regime was found to correlate with the values predicted using the model proposed by Yang [91].

4. The use of mechanically activated fine-grained boron carbide powder complicated the control of synthesis due to burning out of B_4C-Al powder charge during its heating.
5. Depending on processing conditions, the bulk hardness varied between 198 HV10 (as-synthesized) and 809 HV10 (1080 °C, heat treatment in air) for composites with porosity in the range of 2-4 %. For other grades the measured bulk hardness is referred to as an apparent hardness because of high fraction of voids.
6. Secondary processing was found to have a noticeable effect on the flexural strength through a reaction between the initial components. The highest strength was experienced by the composites with the MMC-structure. Vacuum heat treatment drastically reduced the strength because of voids formation. Heat treatment in air resulted in the formation of a quasi-continuous ceramic network that is responsible for the decrease in the flexural strength and ductility of the as-synthesized composite.

   Composites synthesized from fine-grained B_4C powder showed little improvement of the flexural strength as compared with those synthesized from coarse-grained and heat-treated under the same conditions.

Based on results of present work, a processing/microstructure/property map is visualized in Fig. 42.

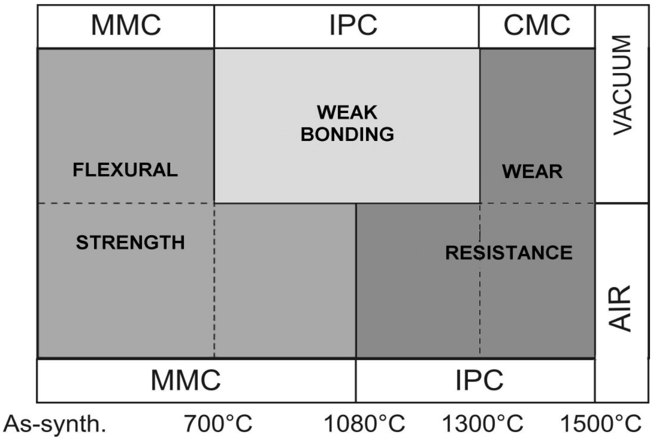

Figure 42. Processing/microstructure/property map for B_4C-Al composites

Suggestions

The combination of reaction synthesis and post-densification heat treatment showed an easy way to produce B_4C-Al composites. Nevertheless, there is room for microstructural optimization through controlling the residual metallic phase content.

Because of open nature of porosity, the composites can be potentially infiltrated to improve the strength.

The optimal refinement of raw B_4C powder should be estimated to obtain the fine-grained composites using SHS.

The effect of each individual Al-B-C phase on the property of composite materials is not understood because of the absence of data about the quantitative composition. The determination of true values of mechanical properties by the extraction of porosity influence for composites with high void fraction is essential for an adequate characterization of performance.

Spontaneous disintegration of composite through hydrothermal processing may provide an alternative way for scrap recycling. From this standpoint, it is important to clarify the interaction of aluminum carbide Al_4C_3 with the environment and other phases in the Al-B-C system.

B_4C-Al composites showed a high wear resistance in dry sliding under the testing conditions of the experiments of present research. However, testing over a broader set of operating conditions is needed to estimate the transition from mild to severe wear for comprehensive characterization of tribological performance.

REFERENCES

1. **K.K. Chawla**. Composite Materials: Science and Engineering. New York: Springer-Verlag, 1987. 483 p.
2. **S.K. Mazumdar**. Composites Manufacturing. Materials, Product, and Process Engineering. Boca Raton: CRC Press, 2002. 416 p.
3. **I.M. Fedorchenko, R.A. Andrievsky**. Fundamentals of Powder Metallurgy. Kiev: Nauk. Dumka, 1963. 420 p. (in Russian).
4. **T. Kishi.** History of materials science and future trends in research. – Materials Science Outlook 2005. National Institute for Materials Science, Japan, 2006.
5. A Vision of Materials Science in the Year 2020. – 2020 NIMS Policy Paper. National Institute for Materials Science, Japan, 2007.
6. **B. Lee, S. Komarneni**. Chemical Processing of Ceramics, 2nd ed. Boca Raton: CRC Press, 2005. 756 p.
7. **Ph. Colomban, G. Gouadec.** The ideal ceramic fiber/oxide matrix composite. How to conciliate antagonist physical and chemical requirements? – Annales de Chemie – Sciences des Materiaux 2005, 30(6), pp. 673-688.
8. **M. Schwartz**. Encyclopedia of Materials, Parts, and Finishes, 2nd ed. New York: CRC Press, 2002. 936 p.
9. **P. Kislij, M. Kuzenkova, N. Bodnaruk, B. Grabchuk**. Boron Carbide. Kiev: Nauk. Dumka, 1988. 216 p. (in Russian).
10. **J.V. Naidich, J.N. Chuvashov**. Wettability and contact interaction of gallium-containing melts with non-metallic solids. – Journal of Materials Science 1983, 18(7), pp. 2071-2080.
11. **C. Manning, T.B. Gurganus.** Wetting of binary aluminum alloys in contact with Be, B_4C, and graphite. – Journal of American Ceramic Society 1969, 52(3), pp. 115-118.
12. **A.J. Pyzik, I.A. Aksay**. Microdesigning of B_4C-Al cermets. – *In*: Proceedings of the International Symposium on Advances in Processing of Ceramic and Metal Matrix Composites, 20-24 August 1989, Halifax, Canada. Pergamon Press, pp. 269-280.
13. **S.-Y. Oh, J.A. Cornie, K.C. Russell.** Wetting of ceramic particulates with liquid aluminum alloys: part I. Experimental techniques. – Metallurgical Transactions A 1989, 20A, pp. 527-532.
14. **S.-Y. Oh, J.A. Cornie, K.C. Russell.** Wetting of ceramic particulates with liquid aluminum alloys: part II. Study of wettability. – Metallurgical Transactions A 1989, 20A, pp. 533-541.
15. **J.C. Viala, J. Bouix, G. Gonzalez, C. Esinouf.** Chemical reactivity of aluminium with boron carbide. – Journal of Materials Science 1997, 32, pp. 4559-4573.
16. **E.C. Lowe.** Process of making boron carbide containing aluminum, and products thereof. – US Patent 2 746 133, 22 May 1956.
17. **O.R. Bergmann**. Cermet of aluminum with boron carbide or silicon carbide. – US Patent 3 178 807, 5 October 1961.

18. **A. Lipp**. Process for the manufacture of a boron, aluminum or alkaline earth metal, and carbon composition and product. – US Patent 3 364 152, 16 January 1968.

19. **D. Halverson, A.J. Pyzik, I.A. Aksay**. Boron-carbide-aluminum and boron-carbide-reactive metal cermets. – US Patent 4 605 440, 12 August 1986.

20. **A.J. Pyzik, P.D. Williams, A. McCombs**. New low temperature processing for boron carbide/aluminum composite armor. Final report. – The Dow Chemical Company. USA. 1990.

21. **G. Arslan, F. Kara, S. Turan**. Quantitative X-ray diffraction analysis of reactive infiltrated boron carbide-aluminum composites. – Journal of the European Ceramic Society 2003, 23, pp. 1243-1255.

22. **G. Arslan, F. Kara, S. Turan**. Reaction model for the boron carbide/aluminium system. – Key Engineering Materials 2004, 264-268, pp. 1059-1062.

23. **K.B. Lee, H.S. Sim, S.Y. Cho, H. Kwon**. Reaction products of Al-Mg/B_4C composite fabricated by pressureless infiltration technique. – Materials Science and Engineering A 2001, 302, pp. 227-234.

24. **D.C. Halverson, A.J. Pyzik, I.A. Aksay**. Processing of boron carbide-aluminum composites. – Journal of American Ceramic Society 1989, 72(5), pp. 775-780.

25. **A.J. Pyzik, D.B. Beaman**. Al-B-C phase development and effects on mechanical properties of B_4C/Al-derived composites. – Journal of American Ceramic Society 1995, 78(2), pp. 305-312.

26. **M. Kouzeli, C. San Marchi, A. Mortensen**. Effect of reaction on the tensile behavior of infiltrated boron carbide-aluminum composites. – Materials Science and Engineering A 2002, 337, pp. 264-273.

27. **M.E. Smagorinski, P.G. Tsantrizos**. Development of light composite materials with low coefficients of thermal expansion. – Materials Science and Technology 2000, 16, pp. 853-861.

28. **A. Grytsiv, P. Rogl**. Aluminum-Boron-Carbon. – Light Metal Systems. Part 1, 11A1. Springer Berlin Heidelberg, 2004, pp. 29-51.

29. **A.R. Kennedy**. The microstructure and mechanical properties of Al-Si-B4C metal matrix composites. – Journal of Materials Science 2002, 37, pp. 317-323.

30. **H.M. Hu, E.J. Lavernia, W.C. Harrigan, J. Kajuch, S.R. Nutt**. Microstructural investigation on B_4C/Al-7093 composite. – Materials Science and Engineering A 2001, 297, pp. 94-104.

31. **T.R. Chapman, D.E. Niesz, R.T. Fox, T. Fawcett**. Wear-resistant aluminum-boron-carbide cermets for automotive brake applications. – Wear 1999, 236, pp. 81-87.

32. **J. Hemanth**. Tribological behavior of cryogenically treated B_4C_p/Al-12% Si composites. – Wear 2005, 258, pp. 1732-1744.

33. **O. Sarikaya, S. Anik, E. Celik, S.C. Okumus, S. Aslanlar**. Wear behavior of plasma-sprayed AlSi/B_4C composite coatings. – Materials and Design 2007, 28, pp. 2177-2183.

34. **J.D. Stachiw, A. Pyzik, D. Carroll, A. Prunier, T. Allen**. Boron carbide aluminum cermets for external pressure housing applications. Technical report. – Naval Command, San Diego, USA, 1992.
35. **B.R. Bart, A.R. Prunier Jr., A.J. Pyzik**. Brake or clutch components having a ceramic-metal composite friction material. – US Patent 6458466, 2002.
36. **T.S Srivatsan, E.J. Lavernia**. Use of spray techniques to synthesize particulate-reinforced metal-matrix composites. Review. – Journal of Materials Science 1992, 27, pp. 5965-5981.
37. **L. Levin, N. Frage, M.P. Dariel**. A novel approach for the preparation of B_4C-based cermets. – International Journal of Refractory & Hard Materials 2000, 18, pp. 131-135.
38. **P.G. Karandikar, M.K. Aghajanian, D. Agrawal, J. Cheng**. Microwave assisted (MASS) processing of metal-ceramic and reaction-bonded composites. – *In*: Mechanical Properties and Performance of Engineering Ceramics and Composites II, Ceramic Engineering and Science Proceedings 2007, 27(2), pp. 435-446.
39. **K.B. Lee, J.P. Ahn, H. Kwon**. Characteristics of AA6061BN composite fabricated by pressureless infiltration technique. – Metallurgical and Materials Transactions A 2001, 32(4), pp. 1007-1018.
40. **L.A. Kommel.** The method of metal/ceramic product manufacturing and container for their manufacturing. – USSR Patent 1836190 A3, 1991.
41. **M.-J. Chao, X. Niu, B. Yuan, E.-R. Liang, D.-S. Wang**. Preparation and characterization of in situ synthesized B4c particulate reinforced nickel composite coatings by laser cladding. – Surface Coatings & Technology 2006, 201, pp. 1102-1108.
42. **A.J. Pyzik, I.A. Aksay**. Multipurpose boron carbide-aluminum composite and its manufacture via the control of the microstructure. – US Patent 4 702 770, 27 October 1987.
43. **J.G.P. Binner**. Advanced Ceramic Processing and Technology. Vol.1. New Jersey, USA: Noyes Publications, 1990. 411 p.
44. **A. Slokombe, L. Li**. Selective laser sintering of TiC-Al_2O_3 composite with self-propagating high temperature synthesis. – *In*: Proceedings of the International Conference on Advances in Materials and Processing Technologies, AMPT'99 and 16th Annual Conference of the Irish Manufacturing Committee, IMC16, 1999, 2, pp. 1261-1269.
45. **J.F. Crider**. Self-propagating high temperature synthesis. http://www.ism.ac.ru/handbook/84crid.htm
46. **A.G. Merzhanov, A.E. Sytschev**. About self-propagating high-temperature synthesis. http://www.ism.ac.ru/handbook/shsf.htm
47. **A.G. Merzhanov**. Self-propagating high-temperature synthesis and powder metallurgy: unity of goals and competition of principles. – *In*: Proceedings of the Powder Metallurgy World Congress, San Francisco, USA, 1992, 9, pp. 341-368.

48. **E.A. Olevsky, E.R. Strutt, M.A. Meyers**. Combustion synthesis and quasi-isostatic densification of powder cermets. – Journal of Materials Processing Technology 2002, 121, pp. 157-166.
49. **S. Torquato, C.L.Y. Yeong, M.D. Rintoul, D.L. Milius, I.A. Aksay**. Elastic properties and structure of interpenetrating boron carbide/aluminum multiphase composites. – Journal of American Ceramic Society 1999, 82(5), pp. 1263-1268.
50. **V.V. Skorohod**. Theory of the physical properties of porous and composite materials and the principles for control of their microstructure in manufacturing processes. – Powder Metallurgy and Metal Ceramics 1995, 34(1-2), pp. 48-63.
51. **A.R. Clarke, C.N. Eberhardt**. Microscopy Techniques for Materials Science. Cambridge, England: CRC Press, 2002. 410 p.
52. **D.R. Clarke**. Interpenetrating phase composites. – Journal of American Ceramic Society 1992, 75, pp. 739-759.
53. **L.D. Wegner, L.J. Gibson**. The mechanical behavior of interpenetrating phase composites – I: modeling. – International Journal of Mechanical Sciences 2000, 42, pp. 925-942.
54. **L.D. Wegner, L.J. Gibson**. The mechanical behavior of interpenetrating phase composites – II: a case study of three-dimensional printed materials. – International Journal of Mechanical Sciences 2000, 42, pp. 943-964.
55. **S. Schmauder**. Computational mechanics. – Annual Review of Materials Research 2002, 32, pp. 437-465.
56. **S. Torquato**. Statistical description of microstructures. – Annual Review of Materilals Research 2002, 32, pp. 77-111.
57. **D.E. Aldrich, Z. Fan**. Microstructural characterization of interpenetrating nickel/alumina composites. – Materials Characterization 2001, 47, pp. 167-173.
58. **X.-Q. Feng, Y.-W. Mai, Q.-H. Qin**. A micromechanical model for interpenetrating multiphase composites. – Computational Materials Science 2003, 28, pp. 486-493.
59. **X.-Q. Feng, Z. Tian, Y.-H. Liu, S.-W. Yu**. Effective elastic and plastic properties of interpenetrating multiphase composites. – Applied Composite Materials 2004, 11, pp. 33-55.
60. **Y. Bao, L. Liu, Y. Zhou**. Assessing the elastic parameters and energy-dissipation capacity of solid materials: a residual indent may tell all. – Acta Materialia 2005, 53, pp. 4857-4862.
61. **K.K. Tho, S. Swaddiwudhipong, Z.S. Liu, K. Zeng**. Simulation of instrumented indentation and material characterization. – Materials Science and Engineering A 2005, 390, pp. 202-209.
62. **W.C. Oliver, G.M. Pharr**. A new improved technique for determining hardness and elastic modulus using load and sensing indentation experiments. – Journal of Materials Research 1992, **7** (6), pp. 1564-1582.
63. XRD JCPDS cards.
64. **J. Jung, S. Kang.** Advances in manufacturing boron carbide-aluminum composites. – Journal of American Ceramic Society 2004, 87(1), pp. 47-54.

65. **J. Bouix, M.P. Berthet, F. Bosselet, R. Favre, M. Peronnet, O. Rapaud, J.C. Viala, C. Vincent, H. Vincent**. Physico-chemistry of interfaces in inorganic-matrix composites. – Composites Science and Technology 2001, 61, pp. 355-362.
66. **C.H. Liu**. Structure and properties of boron carbide with aluminum incorporation. – Materials Science and Engineering B 2000, 72, 23-26.
67. **P. Larsson, N. Axen, S. Hogmark.** Tribofilm formation on boron carbide in sliding wear. – Wear 1999, 236, pp. 73-80.
68. **G.W. Stachowiak, A.W. Batchelor**. Engineering Tribology. Amsterdam: Elsevier Science Publishers, 1993. 872 p.
69. **F. Kreith**. Mechanical Engineering Handbook. Boca Raton: CRC Press, 1999. 2624 p.
70. **D.A. Rigney**. Sliding wear of metals. – Annual Review of Materials Science 1988, 18, 141-163.
71. **D.H. Buckley**. Surface Effects in Adhesion, Friciton, Wear and Lubrication. Amsterdam: Elsevier, 1981. 642 p.
72. **L. Zhou, L. Fang, Y.M. Gao, J.E. Zhou**. The controlling factor in the formation of transfer films on ceramic surfaces during sliding contact against metals. – Tribotest Journal 1996, 3(2), pp. 167-177.
73. **S.K. Biswas.** Some mechanisms of tribofilm formation in metal/metal and ceramic/metal sliding interactions. – Wear 2000, 245, pp. 178-189.
74. **V. Aronov.** Kinetic characteristics of the transformation and failure of the surface layers under dry friction. – Wear 1977, 41, pp. 205-212.
75. **A. Ravikiran**. Wear quantification. – Transactions of the ASME 2000, 122, pp. 650-656.
76. **H. Czichos**. Tribology – A System Approach to Science and Technology of Friction, Lubrication and Wear. Amsterdam: Elsevier, 1978. 416 p.
77. **A. Ramalho, J.C. Miranda**. The relationship between wear and dissipated energy in sliding systems. – Wear 2006, 260, pp. 361-367.
78. **S.L. Donaldson, D.B. Miracle.** ASM Handbook, vol. 21 – Composites. ASM International, 2001. 1100 p.
79. JMicroVision image analysis software. http://www.jmicrovision.com/
80. **M.R. van Landingham**. Review of instrumented indentation. – Journal of Research of the National Institute of Standards and Technology 2003, 108(4), pp. 249-265.
81. **K. Duan, R.W. Steinbrech**. Influence of sample deformation and porosity on mechanical properties by instrumented microindentation technique. – Journal of European Ceramic Society 1998, 18, pp. 87-93.
82. **L.M. Farrissey, P.E. McHugh**. Determination of elastic and plastic properties using indentation: Development of method and application to a thin surface coating. – Materials Science and Engineering A 2005, 399, pp. 254-266.
83. ISO 14577. Instrumented indentation test for hardness and materials parameters.
84. ISO 6507. Vickers hardness test.

85. ASTM E384-05. Standard Test Method for Microindentation Hardness of Materials.
86. ISO 3327. Hardmetals – Determination of Transverse Rupture Strength.
87. ASTM G77. Standard Test Method for Ranking Resistance of Materials to Sliding Wear Using Block-on-Ring Wear Test.
88. **C.A. Queener, T.C. Smith. W.L. Mitchell.** Transient wear of machine parts. – Wear 1965, 8, pp. 391-400.
89. **A.D. Sarkar.** Wear of Metals. New York: Pergamon Press, 1976.
90. **J.F. Archard**. Contact and rubbing of flat surfaces. – Journal of Applied Physics 1953, 24(8), pp. 981-988.
91. **L.J. Yang**. Wear coefficient equation for aluminum-based matrix composites against steel disc. – Wear 2003, 255, pp. 579-592.
92. **K.M. Shorowordi, T. Laoui, A.S.M.A. Haseeb, J.P. Celis, L. Froyen**. Microstructure and interface characteristics of B_4C, SiC and Al_2O_3 reinforced Al matrix composites: a comparative study. – Journal of Materials Processing Technology 2003, 142, pp. 738-743.
93. **J. Guo, G. Liu, Y. Su, J. Jia, H. Fu**. Theoretical calculation of the real vapor pressure of Al during ISM processing of Ni-xAl (at. pct) (x=25~50) alloy. – Journal of Materials Science and Technology 2004, 20(2), pp. 189-192.
94. **V.S. Neshpor, G.P. Zaitsev, S.V. Zhuravlev, A.A. Kitsai, M.A. Aizenberg, V.A. Pesin**. A composite material in the Al-B-C system. – Refractories and Industrial Ceramics 2003, 44(2), pp. 89-91.
95. **M. Rodriguez-Reyes, M.I. Pech-Canul, J.C. Rendon-Angeles, J. Lopez-Cuevas**. Limiting the development of Al_4C_3 to prevent degradation of Al/SiC_p composites processed by pressureless infiltration. – Composites Science and Technology 2006, 66, pp. 1056-1062.
96. **J.K. Park, J.P. Lucas**. Moisture effect on SiC_p/6061 Al MMC: Dissolution of interfacial Al_4C_3. – Scripta Materialia 1997, 37(4), pp. 511-516.
97. **V.L. Solozhenko, E.G. Solozhenko, C. Lathe**. Equation of state and thermal stability of Al_3BC. – Solid State Communications 2006, 137, pp. 533-535.
98. **J**. **Abenojar, P. Diaz, M.A. Martinez, F. Velasco**. Influence of forming on the mechanical properties of the Al + 50% B_4C system. – Materials Science Forum 2006, 530-531, pp. 304-309.
99. **A. Miserez, R. Müller, A. Rossoll, L. Weber, A. Mortensen**. Particle reinforced metals of high ceramic content. – Materials Science and Engineering A 2004, 387-389, pp. 822-831.
100. **A.A Griffith**. Phenomena of rupture and flow in solids. – Philosophical Transactions of the Royal Society of London A 1921, 221, pp. 163-198.
101. **V.P. Bondarenko**. Tribotechnical composites with high-modulus fillers. Kiev: Nauk. Dumka, 1987. 232 p. (in Russian).
102. **G. Arslan, F. Kara, S. Turan**. Mechanical properties of melt infiltrated boron carbide-aluminium composites. – Key Engineering Materials 2002, 206-213, pp. 1157-1160.

103. **V. Imbeni, I.M. Hutchings, M.C. Breslin**. Abrasive wear behavior of an Al_2O_3-Al co-continuous composite. – Wear 1999, 233-235, pp. 462-467.
104. **M.Y. Chen, M.C. Breslin.** Friction behavior of co-continous alumina/aluminum composites with and without SiC reinforcement. – Wear 2002, 249, pp. 868-876.
105. **L. Ceschini, A. Mori, G. Sambogna, M.C. Breslin, M. Fuller**. Microstructure and wear properties of AlSi-Al2O3 and AlSi-SiC-Al2O. – International Journal of Materials and Product Technology 2002, 17(3-4), pp. 165-181.
106. **S. Wang, Y. Wang, C. Li, Q. Chi, Z. Fei.** The dry sliding wear behavior of interpenetrating titanium trialuminide/aluminium composites. – Applied Composite Materials 2007, 14, pp. 129-144.
107. **J. Pirso, M. Viljus, S. Letunovitš**. Friction and dry sliding wear behavior of cermets. – Wear 2006, 260(7-8), pp. 815-824.
108. **J. Pirso, S. Letunovitš, M. Viljus.** Friction and wear behavior of cemented carbides. – Wear 2004, 257, pp. 257-265.
109. **F.T. Cheng, P. Shi, H.C. Man.** Correlation of cavitation erosion resistance with indentation-derived properties for a NiTi alloy. – Scripta Materialia 2001, 45, pp. 1083-1089.
110. **M.Z. Huq, J.-P. Celis.** Expressing wear rate in sliding contacts based on dissipated energy. – Wear 2002, 252, pp. 375-383.
111. **P.-P. Yao, H.-C. Sheng, X. Xiong, B.-Y. Huang**. Worn surface characteristics of Cu-based powder metallurgy brake materials for aircraft. – Transactions of Nonferrous Metals Society of China 2007, 17, pp. 99-103.

LIST OF PUBLICATIONS

1. L. Kommel, R. Traksmaa, E. Kimmari. Influence of binder composition and microhardness on wear properties of lightweight composites. – Powder Metallurgy Progress 2003, 3(3), pp. 140-145. (ISSN 1335-8987).
2. L. Kommel, E. Kimmari. Friction and wear changes of boron carbide cermets depending on structure. – Materials Science (Medžiagotyra) 2003, 9(1), pp. 51-53. (ISSN 1392-1320)
3. L. Kommel, R. Veinthal, E. Kimmari. The formation of structure and change of properties during heat treatment of boron carbide cermets. – Materials Science (Medžiagotyra) 2003, 9(1), pp. 99-101. (ISSN 1392-1320).
4. L. Kommel, E. Kimmari. Recycling of lightweight B_4C based composites. – *In*: Proceedings of the 4th International Conference "Industrial Engineering – New Challenges to SME", Ed. by J. Papstel and B. Katalinic, April 29-30, 2004, Tallinn, Estonia, pp. 199-202.
5. L. Kommel, E. Kimmari. Investigations of structure and tribological properties of the lightweight c-BN-based composites. – Materials Science (Medžiagotyra) 2005, 11(4), pp. 394-397. (ISSN 1392-1320).
6. L. Kommel, E. Kimmari. Boron carbide based composites manufacturing and recycling features. Materials Science (Medžiagotyra) 2006, 12(1), pp. 48 - 52. (ISSN 1392-1320).
7. E. Kimmari, L. Kommel. Application of the continuous indentation test method for the characterization of mechanical properties of B_4C/Al composites. – *In*: Proceedings of the Estonian Academy of Sciences. Engineering, 2006, 4, pp. 399 - 407.
8. L. Kommel, E. Kimmari. Solid Phase's Transformations in Boron Carbide Based Composites during Heat Treatment. Solid State Phenomena 2008, 138, pp. 175-180. (ISSN 1012-0394).
9. E. Kimmari, L. Kommel. Thermally induced cracking in aluminum/boron carbide composite. – *In*: Proceedings of the 6th international conference of DAAAM Baltic industrial engineering, Ed. by R. Küttner, April 24-26, 2008, Tallinn, Estonia, pp. 467-472.

ABSTRACT

Exothermically Synthesized B_4C-Al Composites for Dry Sliding

The development of lightweight wear-resistant materials is of great importance since they provide resource savings. Although boron carbide is known as a lightweight wear-resistant ceramic, very little attention has been paid to B_4C-Al composites as a tribomaterial.

The focus of the present work was to develop the B_4C-Al composites for dry sliding, which were synthesized by the exothermic reaction. Synthesis of composites by the exothermic reaction with subsequent pressing is a cost-effective method of creating lightweight B_4C-Al composite materials. The structure and properties of as-synthesized bodies can be altered by post-densification heat treatment to obtain the composites with high wear resistance in the conditions of dry sliding. Variations in the secondary processing yielded composites with different structure type and a range of mechanical properties.

As a result of the present work the optimal processing parameters for a reaction bonded composite have been proposed to achieve a final desired material suitable for unlubricated sliding.

Keywords: lightweight composite, boron carbide, heat treatment, dry sliding, wear

KOKKUVÕTE

Eksotermiliselt sünteesitud B_4C-Al komposiidid tööks liugehõõrdumise tingimustes

Kergkaaluliste kulumiskindlate komposiitmaterjalide väljatöötamine on tänapäeval ülioluline, sest nende juurutamine aitab kaasa tehnilisele progressile masinaehituses, tagades resursside kokkuhoidu. Kuigi ülikõva boorkarbiid on tuntud kergkaalulise ja kulumiskindla materjalina, seni on vähe töid, mis on suunatud B_4C-Al komposiitide triboomaduste uuimustele.

B_4C-Al komposiidide valmistamise üheks põhiliseks probleemiks on lähtematerjalide suur keemiline aktiivsus, mis raskendab etteantud mikrostruktuuriga komposiitmaterjalide saamise. Tehnilises kirjanduses avaldatud andmed B_4C-Al mikrostruktuuri kujunemise kohta ei ole alati kooskõlas, kuna algmaterjalide keemiline aktiivsus on väga tundlik valmistamisprotsesside tingimustele. Teiseks probleemiks on kõrgtemperatuurse ja pikkaajalise töötluse vajadus B_4C-Al komposiitide saamiseks traditsiooniliste pulbermetallurgia meetoditega (paagutamine, isostaatiline kuumpressimine, infiltreerimine). Antud töös komposiitmetarjalid olid valmistatud eksotermilise sünteesiga patenditud tehnoloogiat kasutades [40], mis võimaldab lahendada eelnimetatud meetodite puudused.

Käesoleva töö eesmärgiks oli välja töötada eksotermiliselt sünteesitud B_4C-Al komposiidid, mis on ette nähtud tööks kuivliugehõõrdumise tingimustes. Selleks sünteesitud materjal oli termiliselt töödeldud erivevatel režiimidel, et saada kergkomposiidid kõrge kulumiskindlusega.

Töö eksperimentaalses osas uuriti termotöötluse mõju saadud materjalide mikrostruktuurile, faasilisele koostisele ja mehaanilistele ning triboloogilistele omadustele. Mikrostruktuursed uuringud viidi läbi OM ja SEMi abil ning XRD ja EDS olid kasutatud faasilise koostise iseloomustamiseks. Mehaanilised omadused määrati indenteerimis- ja paindekatsete abil. Triboomadusi katsetati kuivliugehõõrdumise tingimustes süsteemis komposiit-teras.

Töö tulemused näitasid, et eksotermilise reaktsiooni süntees on sobiv meetod kergkaaluliste (2,1-2,6 g/cm^3) B_4C-Al komposiitmaterjalide tootmiseks. Sünteesitud materjali struktuuri ja omadusi on võimalik parandada järgneva termotöötluse abil. Termotöötlus erinevatel režiimidel vaakumis ja õhu keskkonnas võimaldab luua erineva faasilise koostisega kergkomposiite. On välja pakutud optimaalsed termilise töötluse parameetrid MMC-, IPC-, CMC-tüüpi kulumiskindlate B_4C-Al komposiitmaterjalide saamiseks, mis sobivad tööks kuivliugehõõrdumise tingimustes (vt. Joon. 42).

Antud töö peamisteks järeldusteks on:

1. Kulumiskindlus ja kulumismehhanism on tingitud raua oksiidi Fe_2O_3 sisaldava tribokile moodustumisega komposiidi kulumispinnal. Uuritud

materjalidele on iseloomulik stabiilne hõõrdekoeffitsient vahemikus 0,35-0,45, mis ei muutu hõõrdetemperatuuri kõrgendamisega kuni 200 °C. Kergkaaluliste B_4C-Al komposiitide kulumiskindlus on võrreldav WC- ja TiC-baasil valmistatud kõvasulamite ja kermiste omaga. Kulumise prognoosimine Yang'i [91] mudelit kasutades annab tulemused täpsusega 10 % piires.

2. Termotöödeldud B_4C-Al komposiidi mikrostruktuuri tüüp sõltub keemilise reaktsiooni ulatusest lähtematerjalide vahel ja reaktsiooni põhiprodukti Al_3BC kogusest. Poorsuse tekkimist põhjustavad termotöötlemine vaakumis ja suurema tihedusega faaside moodustumine materjalides.
3. B_4C-Al kermiste mehaaniline tugevus sõltub mikrostruktuursetest näitajatest (poorsus, metalli jääksisaldus, faasiline koostis, mikrostruktuuri tüüp). Suurimat paindetugevust näitasid MMC-struktuuriga ja maksimaalset kõvadust ning kulumiskindlust CMC- ja IPC-struktuuriga komposiidid.

Võtmesõnad: kergkaaluline komposiit, boorkarbiid, termiline töötlemine, kuivliugehõõrdumine, kulumine

CURRICULUM VITAE

1. Personal data

Name	Eduard Kimmari
Date and place of birth	21.09.1977, Kohtla-Järve, Estonia

2. Contact information

Address	Ringi 44-60, Maardu 74112, Estonia
Phone	+372 5560 7170
E-mail	eduard.kimmari@ttu.ee

3. Education

Educational institution	Graduation year	Education (field of study/degree)
Faculty of Mechanical Engineering, Tallinn University of Technology	2003	Product Development and Production Engineering /MSc
Faculty of Mechanical Engineering, Tallinn University of Technology	2001	Product Development and Production Engineering /BSc
Maardu Secondary School	1995	Secondary education

4. Language competence/skills (fluent, average, basic skills)

Language	Level
Estonian	fluent
English	average
Russian	fluent
German	average

5. Special Courses

Period	Educational or other organisation
20-21.10.2005	Welding Standards, Federation of Estonian Engineering Industry
01.12.2005-26.02.2006	Pedagogic and teaching techniques training, Tallinn University of Technology
23-28.10.2006	Design of welded construction with predominantly static loaded moduls of steel structures, German Welding Society (DVS)

26.02-25.06.2007	IIW-course Welding Engineer, German Welding Society (DVS)

6. Professional Employment

Period	Organisation	Position
2005 - …	Tallinn University of Technology	Assistant

7. Scientific work

ETF5611. The technology and properties of lightweight composites. 2003-2004.

T505. Wear resistant materials and wear. 2003-2007.

ETF5878. The technology and properties of nanocrystalline deformable rare metals. 2004-2005.

ETF6163. Nanostructural design of advanced materials. 2005-2008.

ETF6660. Interaction between material particles for engineering new multifunctional (industrial) materials. 2006-2009.

Design and technology of multiphase tribomaterials. 2008-2013.

8. Defended theses

K. Karjakin. BSc. Structure and properties of boron carbide based cermets.

9. Main areas of scientific work/Current research topics

Powder metallurgy, wear and wear-resistant materials.

10. Other research projects

V313. Euroweld. 2005-2007.

ELULOOKIRJELDUS

1. Isikuandmed

Ees- ja perekonnanimi	Eduard Kimmari
Sünniaeg ja –koht	21.09.1977, Kohtla-Järve, Eesti
Kodakondsus	Eesti

2. Kontaktandmed

Aadress	Ringi 44-60, Maardu 74112, Eesti
Telefon	+372 5560 7170
E-posti aadress	eduard.kimmari@ttu.ee

3. Hariduskäik

Õppeasutus (nimetus lõpetamise ajal)	Lõpetamise aeg	Haridus (eriala/kraad)
Mehaanikateaduskond, Tallinna Tehnikaülikool	2003	Tootmistehnika/ teadusbakalaureus
Mehaanikateaduskond, Tallinna Tehnikaülikool	2001	Tootmistehnika/ teadusmagister
Maardu Keskkool	1995	keskharidus

4. Keelteoskus (alg-, kesk- või kõrgtase)

Keel	Tase
Eesti keel	kõrgtase
Inglise keel	kesktase
Vene keel	kõrgtase
Saksa keel	kesktase

5. Täiendusõpe

Õppimise aeg	Täiendusõppe läbiviija nimetus
20-21.10.2005	Keevitusstandardid, Eesti Masinatööstuse Liit
01.12.2005-26.02.2006	Pedagoogika ja õppemetoodika, Tallinna Tehnikaülikool
23-28.10.2006	Staatiliselt koormatud keevituskonstruktsioonide projekteerimine, Saksa Keevitusühing (DVS)
26.02-25.06.2007	Rahvusvahelise/Euroopa keevitusinseneri kursus, Saksa Keevitusühing (DVS)

6. Teenistuskäik

Töötamise aeg	Tööandja nimetus	Ametikoht
2005-…	Tallinna Tehnikaülikool	assistent

7. Teadustegevus

ETF5611. Kergkomposiitide tehnoloogia ja omadused. 2003-2004.

T505. Kulumiskindlad materjalid ja kulumine. 2003-2007.

ETF5878. Deformeeritavate nanostruktuursete haruldaste metallide tehnoloogia ja omadused. 2004-2005.

ETF6163. Kaasaegsete materjalide nanostruktuuri disain. 2005-2008.

ETF6660. Aineosakeste vaheliste vastasmõjude selgitamine multifunktsionaalsete (tööstus-) materjalide väljatöötamiseks. 2006-2009.

Mitmefaasiliste tribomaterjalide arendamine ja tehnoloogia. 2008-2013.

8. Kaitstud lõputööd

K. Karjakin. BSc. Boorkarbiidsete kermiste struktuuri ja omaduste uurimine.

9. Teadustöö põhisuunad

Pulbermetallurgia, kulumine ja kulumiskindlad materjalid.

10. Teised uurimisprojektid

V313. Euroweld. 2005-2007.